remote sensing

MDPI

Article

Integrated Spatiotemporal Analysis of Vegetation Condition in a Complex Post-Mining Area: Lignite Mine Case Study

Jan Blachowski [1,*], Aleksandra Dynowski [1], Anna Buczyńska [1], Steinar L. Ellefmo [2] and Natalia Walerysiak [3]

[1] Faculty of Geoengineering, Mining and Geology, Department of Geodesy and Geoinformatics, Wroclaw University of Science and Technology, 50-421 Wrocław, Poland
[2] Department of Geoscience and Petroleum, Norwegian University of Science and Technology, 7491 Trondheim, Norway
[3] Faculty of Geoengineering, Mining and Geology, Wroclaw University of Science and Technology, 50-421 Wrocław, Poland
* Correspondence: jan.blachowski@pwr.edu.pl; Tel.: +48-71-320-68-75

Abstract: The motivation for this study arises from the need to monitor the condition of a rehabilitated post-mining areas even decades after the end of the recovery phase. This can be facilitated with satellite derived spectral vegetation indices and Geographic Information System (GIS) based spatiotemporal analysis. The study area described in this work is located in Western Poland and has unique characteristics, as it was subjected to the combined underground and open pit mining of lignite deposits that had been shaped by glaciotectonic processes. The mining ended in early 1970'ties and the area was subjected to reclamation procedures that ended in the 1980'ties. We used the Normalized Difference Vegetation Index (NDVI) and the Enhanced Vegetation Index (EVI) spectral indices derived from Sentinel-2 data for the 2015–2022. period. Then, we applied a combination of GIS-based map algebra statistics (local, zonal and combinatorial) and GI* spatial statistics (hot spot and temporal hot spot) for a complex analysis and assessment of the vegetation cover condition in a post-mining area thought to be in the rehabilitated phase. The mean values of NDVI and EVI for the post-mining study area range from 0.48 to 0.64 and 0.24 to 0.31 and are stable in the analyzed 8 year period. This indicates general good condition of the vegetation and post-recovery phase of the area of interest. However, the combination of spatiotemporal analysis allowed us to identify statistically significant clusters of higher and lower values of the vegetation indices and change of vegetation cover classes on 3% of the study area. These clusters signify the occurrence of local processes such as, the encroachment of aquatic vegetation in waterlogged subsidence basins, and growth of low vegetation in old pits filled with waste material, barren earth zones on external waste dumps, as well as present-day forest management activities. We have confirmed that significant vegetation changes related to former mining occur even five decades later. Furthermore, we identified clusters of the highest values that are associated with zones of older, healthy forest and deciduous tree species. The results confirmed applicability of Sentinel-2 derived vegetation indices for studies of post-mining environment and for the detection of local phenomena related to natural landscaping processes still taking place in the study area. The methodology adopted for this study consisting of a combination of GIS-based data mining methods can be used in combination or separately in other areas of interest, as well as aid their sustainable management.

Keywords: underground mining; open pit mining; glaciotectonic; remote sensing; Sentinel-2; GIS; spatial statistics; combinatorial change detection

Citation: Blachowski, J.; Dynowski, A.; Buczyńska, A.; Ellefmo, S.L.; Walerysiak, N. Integrated Spatiotemporal Analysis of Vegetation Condition in a Complex Post-Mining Area: Lignite Mine Case Study. *Remote Sens.* **2023**, *15*, 3067. https://doi.org/10.3390/rs15123067

Academic Editors: Radosław Juszczak, Krzysztof Tajduś and Paweł Ocłoń

Received: 26 April 2023
Revised: 9 June 2023
Accepted: 10 June 2023
Published: 12 June 2023

1. Introduction

1.1. Post-Mining Reclamation

Reclamation is a stage of mining operation focused on creating new or restoring the former use and natural values of an area degraded by extraction of mineral resources [1,2].

Reclamation can be aimed at reforestation, agriculture, creation of artificial water bodies (in flooded open pits), creation of recreational sites or a combination of these land uses [1,3,4]. Sometimes the post-mining sites are left to natural landscaping processes [5,6].

The number of post-mining areas worldwide is growing and requires effective and reliable methods of monitoring their condition. Kretschmann & Nguyen [7] argue that the processes affecting the post-mining environment are continuous and should be treated as eternal tasks. Therefore, post-mining sites should be subjected to permanent monitoring [8], also in the rehabilitated phase. However, it is often limited in scope or neglected in time due to, among other things, high costs of such procedures.

In terms of the condition of the environment, Yang et al. [9] identify two change points in a mine operation life cycle. These are the start of the environment disturbance (t_1) caused by mining and the beginning of environment recovery (t_4) with the introduction of reclamation and development procedures. In addition, a point of disturbance to post-mining recovery of the environment can occur (t_5) due to potential secondary effects of mining, e.g., secondary subsidence [10] or incorrect reclamation measures [7,9]. These change points have been illustrated in Figure 1. In our study we focus on the rehabilitated phase of the mine life cycle.

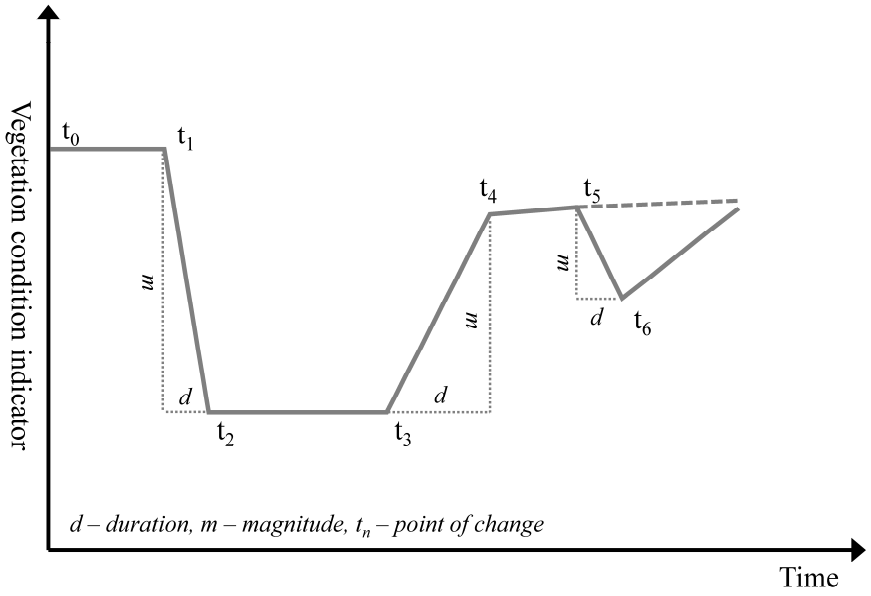

Figure 1. Vegetation condition trajectory in time at a mining site (after Yang et al. [9], modified), t_0—initial condition, t_1—start of mining disturbance, t_2—mining operation phase, t_3—start of rehabilitation, t_4—end of rehabilitation phase, t_5—occurrence of post-mining disturbance, t_6—start of secondary recovery.

1.2. Remote Sensing of Post-Mining Areas

The assessment of the post-mining environment is most often focused on spatiotemporal analysis of vegetation, water or soil conditions. Traditional field monitoring methods are usually limited to small areas and characterised with low frequency due to the high costs of in-situ measurements. This approach results in an incomplete picture of the processes of mine disturbance and rehabilitation of the environment [9,11]. Remotely sensed data acquired by satellite and airborne platforms such as Unmanned Aerial Vehicles (UAVs) provide a practical and cost-effective solution for monitoring mining disturbance and rehabilitation of entire post-mining areas with high spatial and temporal resolution [12,13]. Publicly available open satellite imagery of the Landsat and Sentinel-2 missions already have been widely and effectively used for assessing, tracking and historical reconstruction of the environmental conditions and changes in different areas of interest based on analysis of various spectral indices. For example, vegetation spectral indices are considered

an indispensable tool in classifying land cover and long-term monitoring of vegetation changes taking place in various areas, e.g., agriculture land, forest management [14]. Bannari et al. [15] provide comprehensive and well-established chronological overview of vegetation spectral indices applied in the analysis and monitoring of vegetation cover starting from the indices proposed by Pearson and Miller [16], i.e., the Ratio Vegetation Index (RVI) and the Vegetation Index Number (VIN). The review ends with the Modified Soil Adjusted Vegetation Index (MSAVI) and the Angular Vegetation Index (AVI) described in [17,18], respectively. Xue and Su [19], based on 138 references, provide an alphabetical list of as many as 118 vegetation indices with their concise characteristics. A database with basic characteristics of vegetation spectral indices has been developed by Henrich et al. [20] and is available at the www.indexdatabase.de webpage (accessed on 22 September 2022).

With regard to monitoring and assessment of vegetation cover condition in post-mining areas with the use of satellite remote sensing imagery Pawlik et al. [21] have prepared a review of vegetation indices used for studies of processes in former-mining environments based on 92 scientific publications published between 1968 and 2020. This review lists chronologically and concisely describes 42 indices.

In an another study Buczyńska [22] classifies satellite spectral indices that are used for monitoring of post-mining areas into four categories: vegetation indices, geological indices, indices used for determining the water content in soils and indices designed to identify areas damaged by fires. In the first group the author lists 13 indices.

The authors of above publications state that vegetation indices (Vis) obtained from remote sensing have been used in different applications, one of which is monitoring of mining and post-mining areas. According to Xue and Su [19] Vis are simple and effective algorithms for quantitative and qualitative evaluations of vegetation cover, vigour, and growth dynamics. Noteworthy, recent studies utilising satellite imagery in mining area studies and listed chronologically include works by: Zipper et al. [23]; Karan et al. [24]; Yao & Wei [25]; Padmanaban et at. [26]; Yang et al. [9]; Li et al. [27]; Wu et al. [28]; Kopeć et al. [29]; Vidal-Macua et al. [30]; Vorovencii [31]; Guan et al. [32]. A brief summary of their findings has been given below. Zipper et al. [23] have assessed mine land disturbance and reclamation process over a 27-years period for the Wise County Appalachian coal field (USA) with time series analysis of the Normalized Difference Vegetation Index (NDVI) calculated from Landsat data. Karan et al. [24] have assessed the reclamation process of coal post-mining area in India based on NDVI and the Enhanced Vegetation Index (EVI), as well as linear regression and support vector machine (SVM) approach. Yang et al. [9] have assessed the applicability of the LandTrendr algorithm to detect trajectory of the vegetation change for the Curragh coal mine site in Australia based on analysis of the Landsat derived NDVI for the 1988–2015 period. Li et al. [27] have analysed land cover distribution, mining area damage and recovery process based on the Landsat 5 and Landsat 8 derived NDVI between 1990–2016 for the Lingbei rare earth mine in China. Yao and Wei [25] have assessed changes in vegetation condition of a reclaimed mining area in China through time series analysis of 19 vegetation indices, including NDVI and EVI and principal component analysis (PCA). Padmanaban et al. [26] have applied Landsat imagery from 2013–2016 to analyse land cover dynamics, and the increase of wetland areas over the Kirchheller Heide mine in Germany. The authors have applied Spectral Mixture Analysis (SMA) of NDVI. Wu et al. [28] have proposed an algorithm to detect mining activity and assess the spatial distribution of the affected vegetation based on the NDVI index derived from MODIS and Landsat data. Kopeć et al. [29] have combined Sentinel-1 interferometric and Sentinel-2 NDVI and MNDWI data with geographically weighted and random forest regression methods to assess the potential of wetland formation over an active underground coal mining area in Poland. Vidal-Macua et al. [30] have combined Landsat satellite data time series analysis of the NDVI and machine learning technique to identify suitable conditions for vegetation development in reclaimed open-cast mines for a case study of Teruel coalfield in central-eastern Spain. Vorovencii [31] has used Landsat imagery for the years 1988, 1998, 2008, and 2017 to map the extent of surface mining and

reclamation in the Jiu Valley (Romania). The author used NDVI, Soil-Adjusted Vegetation Index (SAVI), and Modified Soil-Adjusted Vegetation Index-2 (MSAVI-2) to classify land cover types. Guan et al. [32] have used the NDVI time series data, filter processing and logistic function to analyse the succession characteristics of rehabilitated vegetation for a dump of open-cast coal area in China. They have concluded that the average development period for new vegetation to reach a stable state is 13 years.

The main topics of post-mining studies that used high-resolution, satellite multispectral imagery covered: classification of land use types and separation of areas covered with vegetation, determination of the range of mining operations, changes in the condition of the vegetation over time, determination of the moment of restoration of the vegetation state, to that known before the exploitation, and determination of subsidence zones and their impact on vegetation degradation. The analytical algorithms used most often for these applications included: spatiotemporal statistics [9,23,33], multivariate global and local spatial regression models [29], e.g., for analysis of the relationship between ground subsidence and potential causative factors [34–36], supervised and unsupervised machine learning algorithms [30], e.g., for land cover change analysis [37], land cover classification [38], damage assessment, monitoring and land management [39], quantification of land cover change following closure of an open-pit mine with limited reclamation [40], estimation of reforestation progress above a reclaimed mine [41].

1.3. Summary

Until recently, the studies of the condition of the environment in mining and post-mining areas were based largely on the Landsat missions' data. The number of studies based on the Copernicus Sentinel-2 mission that operates from 2015 is yet lower. However, the Sentinel-2 mission offers better temporal (5 days revisit time for most of the Earth surface), and spatial resolution of 10 m as compared to 30 m for the Landsat data [42]. Xue and Sue, [19] point out the following advantages of satellite based remote sensing: free access to visible and multispectral data (in case of the above mentioned missions), high spatial resolution, possibility to extract long time series of consistent and comparable data, cost effectiveness as compared to field sampling. The limitations may be caused by observations in cloudy conditions, recommendation to verify the results in the field, as well as low pixel resolution and revisit times for some applications, e.g., farming.

Among the vegetation spectral indices used in the studies presented in the reviewed publications, the most frequently chosen for mining areas was the NDVI. The second most often used being the EVI. The first index was used, e.g., to designate areas with different vegetation conditions, the second to provide information on structural changes in flora, e.g., vegetation species differentiation.

The literature review, presented above and based on query of the Scopus, Web of Science and Google databases indicates that the number of published studies on vegetation condition assessment decades after the end of mining and past the recovery phase is very limited. The same conclusion applies to the use of a combination of advanced GIS-based spatial statistics functions. We have not found a study related to the assessment of the vegetation condition in a rehabilitated post-mining area characterised by a combined, underground and open pit mining of lignite.

Thus, the main objective of this study has been to analyse and to assess vegetation (forest) condition in a complex lignite post-mining area nearly five decades after the end of mining and presently thought to be in the rehabilitated phase. For this purpose, we chose and adapted complementary Geographic Information System (GIS) based spatiotemporal statistics that included: map algebra functions (local and zonal), temporal Hot Spot analysis and combinatorial class change detection analysis. These were applied to a time-series of satellite derived imagery. The research has been carried out for the case study of a former underground and open-cast lignite mine located in a topography transformed by glacio-tectonic processes (Western Poland bordering with Germany). Based on the results of literature review we used the NDVI and the EVI spectral indices derived from the European

Copernicus programme Sentinel-2 mission. The analysis covered the period from 2015 to 2022.

2. Materials and Methods

2.1. Study Area

This study covers the area of a rehabilitated part of the former lignite mine "Przyjaźń Narodów—Szyb Babina" in Western Poland.It is situated in the south-east part of the glaciotectonic landscape called the Muskau Arch between 51°30′–51°36′N and 14°42′–14°50′E. Its location is shown in Figure 2. The specific study area covers 13.78 km^2 (Figure 3). The arch is a geomorphological structure in the form of a terminal moraine shaped by an ice sheet lobe from the South Polish (Elsterian) glaciation. The formation is visible in the morphology of the terrain as semicircular hills separated by elongated depressions. Its arms span approx. 20 km and have length of approx. 40 km with width of around 5–6 km [43,44]. The Muskau Arch is divided by the Nysa Łużycka river that also constitutes the Polish-German boundary.

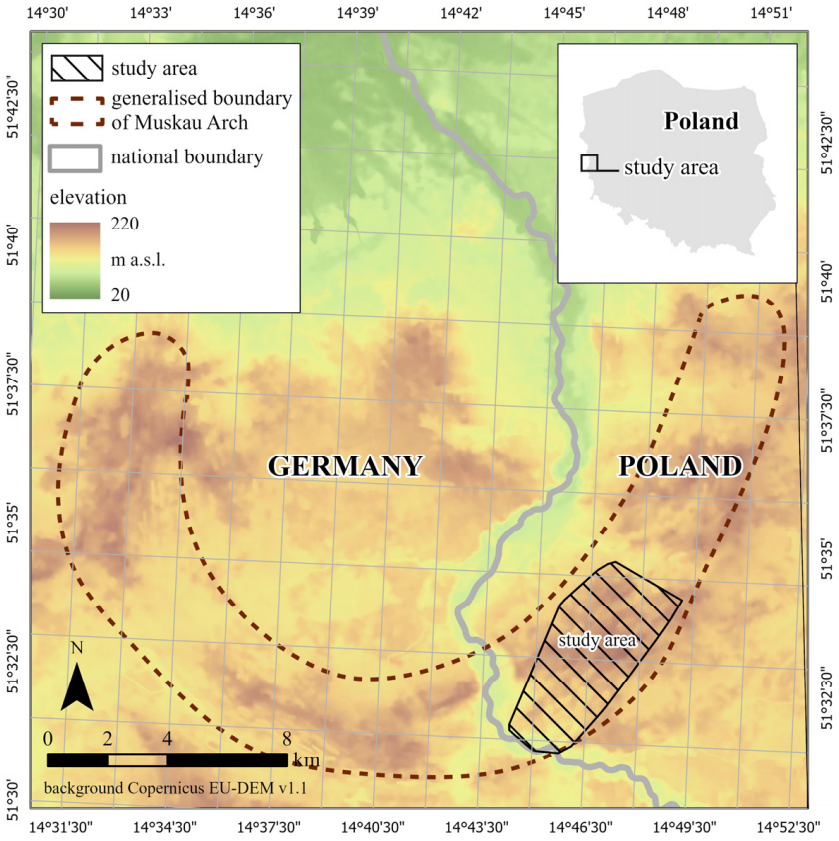

Figure 2. Location of the study area.

The glaciotectonic deformations of Neogene formations, such as lignite, sand and clay sediments are visible in morphology, as well as in data from geological boreholes and mining excavations. These structures were forced towards the surface by the moving ice sheet and formed glaciotectonic scale-like features accompanied by fold-like structures and diapirs [45].

The lignite deposits shaped by these processes were subjected to long-term mining, first with underground and later with open pit methods. The mine operated from 1921 to 1973. The first small open pits functioned between 1935 and 1940. Open cast mining was introduced on a larger scale from the 60'ties of the 20th Century. It is estimated that altogether 479 ha of land was transformed by underground and open pit activities [46,47]. Until 1966, the mining company carried out technical reclamation on an area of approx.

30 ha that was exploited during the World War II, between 1940 and 1944. The main rehabilitation of post-mining grounds started in the early 70'ties. The process was aimed at afforestation of external and internal dumps, as well as zones adjacent to old open pits, and creation of artificial lakes by filling the abandoned pits with water [48]. Planting of various tree species, such as pine, aspen, birch and oak was preceded by technical preparation of the terrain (e.g., levelling). The afforestation procedures were carried out on grounds with low pH (below 3.0), without proper treatment with neutralizers and enrichment with mineral fertilisers [47]. Thus, the substrate used for planting vegetation formed a loose environment made of fine-grained and dusty Miocene sands, often with lignite fractions. In the effect, the post-mining area was subjected to water erosion and deflation that had destructive effects on the planted fauna, especially on the slopes and lower lying zones. This, in consequence, caused secondary degradation of the post-mining site and reclamation procedures were repeated in the first half of the 80'ties of 20th Century [46].

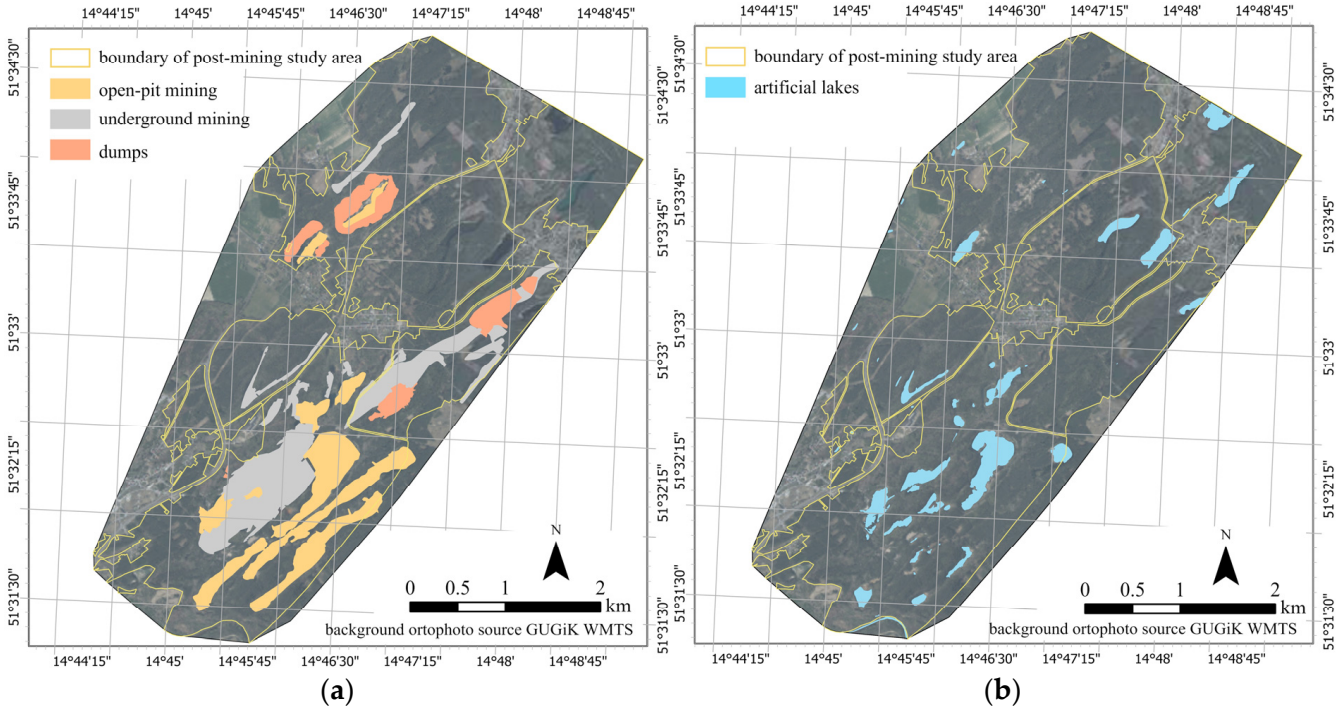

Figure 3. The known extent of underground and open pit mining (**a**), present-day artificial lakes (**b**) against the background of aerial imagery.

As a result of first mining and then reclamation, the primeval post-glacial landscape has been transformed with the post-mining reservoirs filled with acidified and sulphated waters. These reservoirs are the main anthropogenic feature of the transformed landscape [47,49] and have depths ranging from several to over a dozen meters, with the area of largest lake over 20 ha.

Apart from artificial lakes and dumps, the following anthropogenic landforms can be distinguished in the area: subsidence basins of irregular, usually elongated shape, occurring over old underground workings, sometimes forming waterlogged wetlands; circular sinkholes, several metres in diameter and depth, created in the process of loose deposits moving into voids left by shallow underground mining, usually due to hydraulic processes in the ground [50]; larger and deeper sinkholes in the vicinity of old shafts usually filled with water [45,51].

The known extent of open-pits, dumps and underground mining, interpreted from cartographic documents [50] is presented on the orthophoto background in Figure 3a. Figure 3b shows the location of present-day artificial lakes.

2.2. Data

2.2.1. Sentinel-2 Data

In our study we have employed multispectral imagery captured by the European Space Agency Copernicus Sentinel-2 mission. The Multi Spectral Instrument (MSI) Level-1C (L1C) products were downloaded from the U.S. Geological Survey (USGS) EarthExplorer data portal (https://earthexplorer.usgs.gov/ (accessed on 22 September 2022)). We have inspected and selected cloud free images registered in the month of August from 2015 to 2022 to represent vegetation cover in the same phenological phase. The dates of acquisition of satellite imagery used for the analyses are given in Table 1.

Table 1. List of the images selected for this study and their acquisition dates.

Year	Month	Day
2015	August	20
2016	August	27
2017	August	29
2018	August	27
2019	August	29
2020	August	6
2021	September *	5
2022	August	16

*—no cloud free August image is available for the study area in 2021.

We chose the Sentinel-2 data for the following reasons. First, it has been in service since 2015 and provides sufficient observation time to assess the vegetation condition of the study area in the post-rehabilitation stage we aimed at. Second, the spatial resolution of Sentinel-2 products (pixel size of 10 m) provides a good framework for monitoring vegetation change in the post-mining environment. Other open source satellite imagery, such as the Landsat mission provides data with lower, 30 m pixel resolution.

2.2.2. GIS Data and Software

The GIS data used in this study comprised of polygon feature vector layers characterising present day land cover types available from the Polish national database of topographic objects provided by the regional office for geodetic and cartographic documentation (https://wodgik.lubuskie.pl/bdot10k (accessed on 22 September 2022)), polygon feature vector layers representing forest units available from the National Forest Data Bank (https://www.bdl.lasy.gov.pl/portal/mapy-en (accessed on 22 September 2022)), and polygon feature vector layers representing extent of underground and open pit mining and post-mining and geological features obtained from the Polish Geological Institute—National Research Institute [50] and updated under the Polish National Science Centre OPUS project no 2019/33/B/ST10/02975 [51]. The GIS data processing and spatiotemporal analyses have been performed in ESRI ArcGIS Pro software v. 2.8 licensed to the Wroclaw University of Science and Technology (subscription ID 1133081784) and Python scripts.

2.3. Methodology

The integrated methodological approach adopted for analysis and assessment of vegetation cover condition in a post-mining area in our study is presented in Figure 4. and summarised in the succeeding subsections.

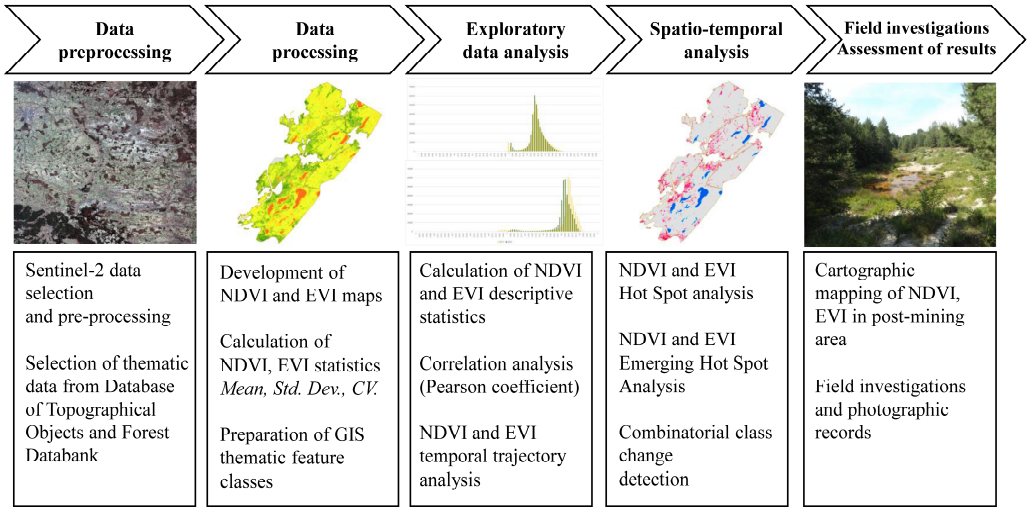

Figure 4. Methodology of the research.

2.3.1. Satellite Data Pre-Processing

The acquired Sentinel-2 images in the L1C processing level (top-of-atmosphere reflectance (TOA) in cartographic geometry) were converted to the L2A product, in which individual pixels of the image store information about the value of the bottom-of-atmosphere reflectance (BOA) [42]. The conversion between L1C and L2A products included scene classification and atmospheric correction [52], which were performed in SNAP 8.0 software using the Sen2Cor processor (2.8.0 version), developed by Mueller-Wilm et al. [53]. The pre-processed images were used to determine two vegetation indices: NDVI and EVI.

The methodology for deriving the NDVI and EVI spectral indices from satellite images has been widely described in various publications [24,26,31,54,55]. Below we summarise the main steps, providing literature for the readers less familiar with remotely sensed data processing.

NDVI is the most commonly used vegetation index, developed by Rouse et al. [56]. It is a combination of red and near-infrared bands, thus the spectral ranges in which the highest absorption and reflection of solar radiation by vegetation are observed, respectively [57,58]. The NDVI index is given by the Formula (1):

$$NDVI = \frac{NIR - RED}{NIR + RED} \quad (1)$$

where, RED and NIR represent the spectral reflectance values in the red and near infrared bands, respectively (NIR spectral range is represented by band 8 and RED spectral range is represented by band 4 of the Sentinel-2 mission).

The NDVI takes values from −1 to 1 and is used for assessment of the general condition of vegetation and its identification among other forms of land cover [24]. Negative values of the index prove the lack of flora in a given region, while values in the range from 0.2 to 0.8 are typical for areas covered with vegetation. The highest NDVI values (more than 0.8) indicate a dense and healthy plant cover [59]. It is worth to emphasize that this index is sensitive to the effects of soils, atmosphere and shadows [60].

EVI was developed to improve the accuracy of vegetation studies in areas of high biomass. The index is described by the Formula (2) [61]:

$$EVI = G * \frac{NIR - RED}{NIR + C_1 * RED - C_2 * BLUE + L} \quad (2)$$

where,

BLUE—value of spectral reflectance in the blue band,

G—gain factor (*G* = 2.5),

L—canopy background adjustment (L = 1.0),
C_1, C_2—coefficients of the aerosol resistance term (C_1 = 6.0, C_2 = 7.5).

EVI reduces the effects of the atmosphere and soil background by application of the blue band [62]. This index takes values from −1 to 1. As in the case of NDVI, negative values of the EVI index indicate areas devoid of vegetation, while high positive values represent healthy and dense flora [63].

Both vegetation indices were calculated using the dedicated band indices and map algebra toolboxes in ESRI ArcGIS Pro v.2.8.0.

2.3.2. GIS Based Spatiotemporal Analysis

We have combined the Getis-Ord Gi* spatial statistic based temporal hot spot and map algebra based spatial statistics approach for the complementary spatiotemporal analysis and assessment of vegetation condition in the rehabilitated stage of the post-mining area. In addition, we integrated map algebra local, zonal and combinatorial raster functions for data pre-processing, exploratory analysis, reclassification and vegetation class change detection.

- Map algebra

We used the map algebra [64] raster cell functions to calculate the following spatial statistics for individual locations (pixels): mean value, range, standard deviation, and coefficient of variation for the stack of rasters representing NDVI and EVI values from August 2015 to August 2022. Coefficient of variation (CV) is the ratio of the standard deviation σ to the mean μ (3) [65].

$$CV = \frac{\sigma}{\mu} \tag{3}$$

It presents the extent of variability in relation to the mean value of the data. Thus, the higher the coefficient of variation, the greater the level of dispersion around the mean.

For the correlation analysis on a pixel by pixel level, we applied the Pearson correlation coefficient (r), which is used to measure the strength of a linear association between two variables (4) [65].

$$r = \frac{\sum_{i=1}^{n}(x_i - \overline{x})(y_i - \overline{y})}{\sqrt{\sum_{i=1}^{n}(x_i - \overline{x})^2}\sqrt{\sum_{i=1}^{n}\left(y_i - \overline{y}\right)^2}} \tag{4}$$

where,

r is the Pearson correlation coefficient,
x_i is the value of the variables x,
y_i is the value of the variable y,
$\overline{x}$ is the arithmetic mean of variable x,
$\overline{y}$ is the arithmetic mean of variable y.

- Combinatorial class change detection

For the temporal land cover change detection analysis, we first applied raster reclassification function to classify the floating-point NDVI and EVI values into categorical maps representing land cover classes.

We assigned the following classes for NDVI data:

- class 1: NDVI $\leq$ 0.0—representing water,
- class 2: 0.0 < NDVI $\leq$ 0.2—representing barren land, roads and sparse vegetation,
- class 3: 0.2 < NDVI—representing low vegetation and forest.

For EVI data we used the following classes:

- class 1: EVI $\leq$ 0.0—representing water,
- class 2: 0.0 < NDVI $\leq$ 0.1—representing barren land, roads and sparse vegetation,
- class 3: 0.1 < EVI—representing low vegetation and forest.

The boundary values have been chosen based on literature review and verification of the above described conditions for randomly selected 18 ground control points, 6 in water area, 4 in barren land area and 10 in vegetation/forest zones.

Next, we used the combinatorial map algebra functions to detect vegetation temporal change by assigning new values to each unique combination of input classes in the compared raster stack. The general procedure is illustrated in Figure 5 on the example of 2 input raster datasets with three vegetation cover categories.

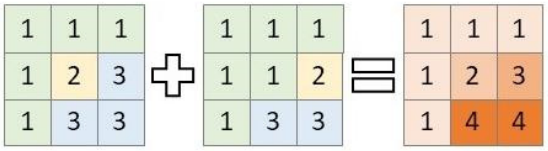

Figure 5. Illustration of the combinatorial change detection method, compared classified raster datasets (**left**), result of combinatorial operation (**right**).

For both spectral indexes we obtained 9 possible combinations:

- 1—change from class 1 to class 2,
- 2—change from class 1 to class 3,
- 3—change from class 2 to class 3,
- 4—change from class 2 to class 1,
- 5—change from class 3 to class 2,
- 6—change from class 3 to class 1,
- 7—unchanged class 1,
- 8—unchanged class 2,
- 9—unchanged class 3.

To record the change in the stack of analysed raster layers, the identified combinatorial change, once it happened, had to be permanent or last for at least 2 epochs in case of the last two periods.

- Emerging Hot Spot Analysis

The Getis-Ord Gi* spatial statistic algorithm available in GIS software is widely used for hot spot analysis [10,66]. By calculating the Gi* statistic of spatial features (spatial variable), it is possible to identify the clustering of zones with high (hot spot) and with low (cold spot) values of a spatial variable in the context of their neighbourhood. The theory behind this analysis has been described in [67,68]. The calculation is based on the Formula (5) [67].

$$G_i^* = \frac{\sum_{j=1}^{n} w_{i,j}x_j - \overline{X}\sum_{j=1}^{n} w_{i,j}}{S\sqrt{\frac{\left[n\sum_{j=1}^{n} w_{i,j}^2 - \left(\sum_{j=1}^{n} w_{i,j}\right)^2\right]}{n-1}}} \quad (5)$$

where:

x_j—variable value for feature j,
$w_{i,j}$—spatial weight between feature i and j,
n—total number of features,
$\overline{X}$ is given by Equation (6),
S—is given by Equation (7):

$$\overline{X} = \frac{\sum_{j=1}^{n} x_j}{n} \quad (6)$$

$$S = \sqrt{\frac{\sum_{j=1}^{n} x_j^2}{n} - \left(\overline{X}\right)^2} \quad (7)$$

When the analyzed data are a timeseries, the hot spot analysis can identify the changing trend of the data [66,69]. The emerging hot spot analysis has been successfully applied

in studies of vegetation condition based on the NDVI satellite derived spectral index in a river basin in China [66], impact assessment of watershed development in India [70], temporal and spatial variation of vegetation in an economic development belt in China [71], drought area analysis in Iran [72] with one of the first applications by Fraser et al. [73] for identification of forest burned area in Canada.

Using the calculated NDVI and EVI values as input data, we calculated the standard deviations and probability values for each location (pixel). We used these values, standard deviations < −2.58 or >+2.58 with associated probability values < 0.01 (99% confidence level) and standard deviations < −1.96 or >+1.96 with associated probability values < 0.05 (95% confidence level) to determine clusters of locations with statistically significant high and low values of these variables in the 2015–2022 period. In the temporal hot spot approach, we checked each location (pixel) for a potential change of the hot or cold post on a step-by-step basis. In the result, we mapped the stable hot and cold spots, as well as the emerging hot and cold spots—locations, for which the statistical values changed over time in the rehabilitated post-mining study area.

3. Results

3.1. General Descriptive Statistics

First, we present the general descriptive statistics for the post-mining study area as background information for spatial analysis of the NDVI and EVI vegetation indices distribution and temporal changes.

The mean values of the NDVI spectral index in the study area calculated for the selected dates in August (Table 1) range from 0.48 to 0.64. The mean NDVI values in the study area excluding artificial lakes, that are represented by negative and very low (close to zero) values of NDVI, range from 0.50 to 0.68 (Table 2, Figure 6).

Table 2. General descriptive statistics for the NDVI spectral index for the post-mining study area and for the post-mining study area without artificial lakes.

Date	With Artificial Lakes				Without Artificial Lakes			
	Min	**Max**	**Mean**	**Std Dev.**	**Min**	**Max**	**Mean**	**Std Dev.**
August 2015	−0.16	0.78	0.56	0.13	−0.10	0.79	0.59	0.08
August 2016	−0.42	0.87	0.64	0.17	−0.33	0.87	0.68	0.09
August 2017	−0.36	0.83	0.62	0.16	−0.26	0.83	0.65	0.09
August 2018	−0.21	0.78	0.57	0.13	−0.07	0.78	0.60	0.08
August 2019	−0.07	0.72	0.48	0.10	0.06	0.72	0.50	0.07
August 2020	−0.03	0.73	0.52	0.10	0.07	0.73	0.53	0.07
August 2021	−0.23	0.82	0.61	0.13	0.03	0.82	0.63	0.07
August 2022	−0.40	0.83	0.61	0.15	−0.03	0.83	0.64	0.08

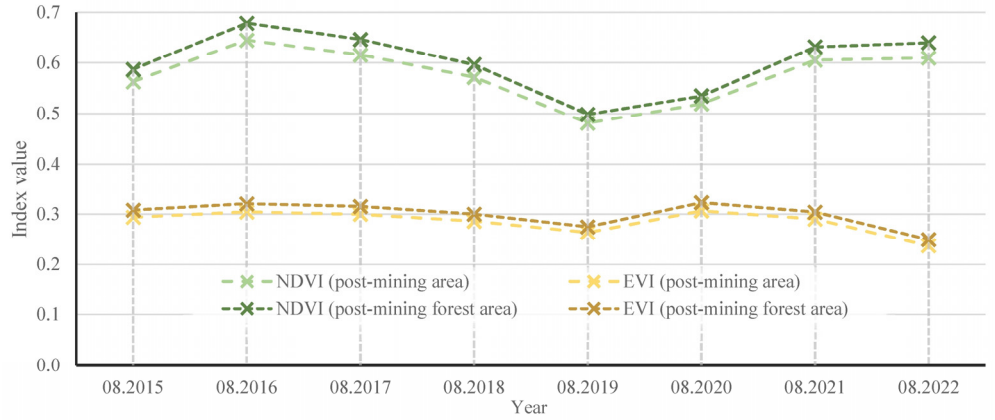

Figure 6. Temporal trajectory of the NDVI and the EVI values in the post-mining study area and the post-mining study area excluding artificial lakes.

The mean values of the EVI spectral index in the study area calculated for the same dates range from 0.26 to 0.30. Whereas the EVI values in study area excluding artificial water bodies range from 0.28 to 0.32 (Table 3, Figure 6).

Table 3. General descriptive statistics for the EVI spectral index for the post-mining study area and for the post-mining study area without artificial lakes.

Date	With Artificial Lakes				Without Artificial Lakes			
	Min	Max	Mean	Std Dev.	Min	Max	Mean	Std Dev.
August 2015	−0.05	0.64	0.29	0.09	−0.02	0.64	0.31	0.07
August 2016	−0.12	0.78	0.30	0.10	−0.06	0.78	0.32	0.08
August 2017	−0.10	0.67	0.30	0.10	−0.06	0.67	0.32	0.08
August 2018	−0.06	0.59	0.29	0.09	−0.01	0.59	0.30	0.07
August 2019	−0.03	0.54	0.26	0.07	0.02	0.54	0.27	0.05
August 2020	−0.10	0.69	0.31	0.10	−0.02	0.69	0.32	0.08
August 2021	−0.05	0.63	0.29	0.09	0.01	0.63	0.30	0.07
August 2022	−0.08	0.53	0.24	0.08	0.00	0.53	0.25	0.06

The temporal trajectory of the mean NDVI and EVI values in the post-mining study area is presented graphically in Figure 6. The highest mean NDVI values occurred in 2016 and steadily decreased between 2017 and 2019 when they were at the lowest. In the 2020–2022 period the mean NDVI values steadily increased each year.

The highest mean EVI values were registered in 2016, as in the case of NDVI and in 2020. The calculated mean EVI values steadily decreased between 2017 and 2019 similarly to the mean NDVI values. However, after the peak in 2020, in the 2021–2022 period there was a decrease in the mean EVI values, unlike in case of the other index.

The graph shown in Figure 7 represents the measure of correlation between mean NDVI and mean EVI values in the 2015–2022 period. The calculated Pearson correlation coefficient, which is used to measure the strength of a linear association between two

variables [74] ranges from 0.75 for the 2020 data to 0.92 for the 2019 data. The range of these values indicates a strong correlation between the two spectral indices (we should note that the NIR and the RED spectral bands are used to calculate values of both indexes).

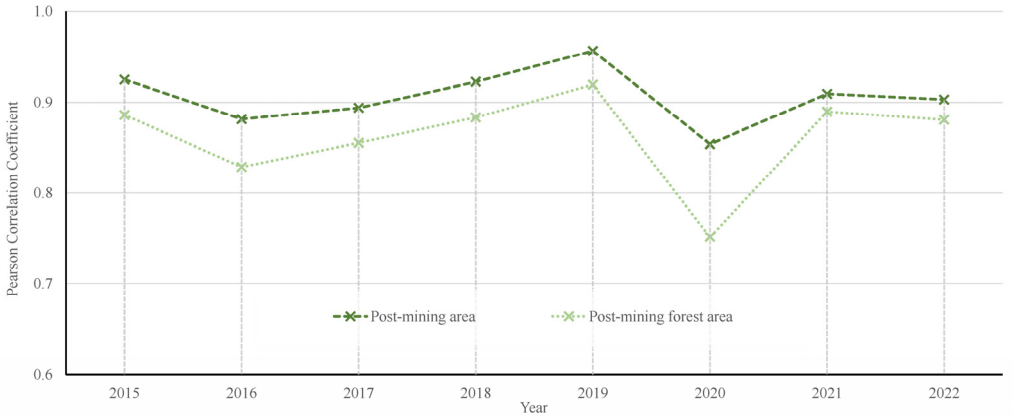

Figure 7. Pearson coefficient of correlation between the NDVI and the EVI values for the 2015–2022 period.

Figures 8 and 9 are the histograms of NDVI and EVI pixel values for the first period (2015) and for the last period (2022) binned in 0.02 intervals. The histogram of NDVI values for the post-mining area has negative skewness for the 2015 data (−2.70) and for the 2022 data (−2.44). The shift of the histogram values to the left between 2015 and 2022 points to a potential general weakening of the condition of the forest vegetation in the analysed period and represented by this spectral index. We interpret, the shift to the right (negative to positive values, and lower to higher values) of the slight "bulge" in the left tail of the histogram as potential natural landscaping processes taking place in local zones of the study areas, such as decrease of the surface water area, emergence of aquatic vegetation in artificial lakes and appearance of low vegetation in barren parts of mining dumps.

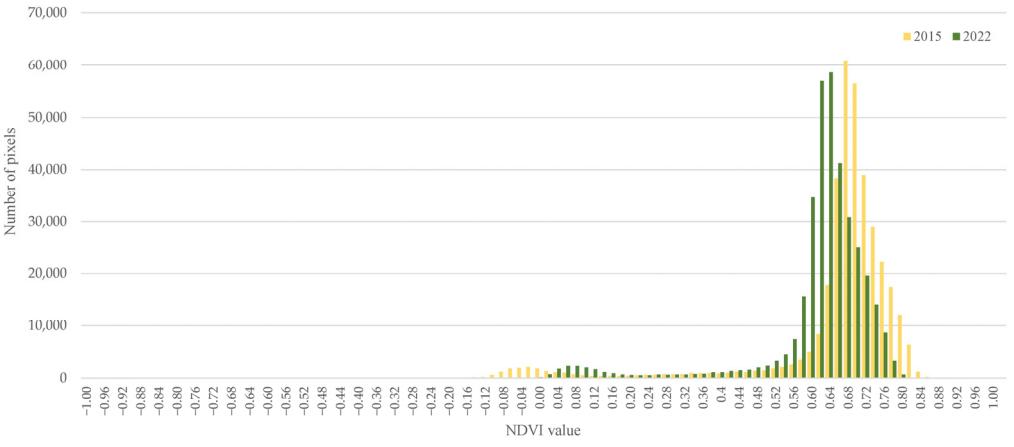

Figure 8. Histogram of the NDVI values for the 2015 and for the 2022 data.

This shape of the NDVI histograms is generally repeated for the 2015 and 2022 histograms of the EVI values (Figure 9). However, the factor of skewness is lower, as well as the smaller factor of the shift.

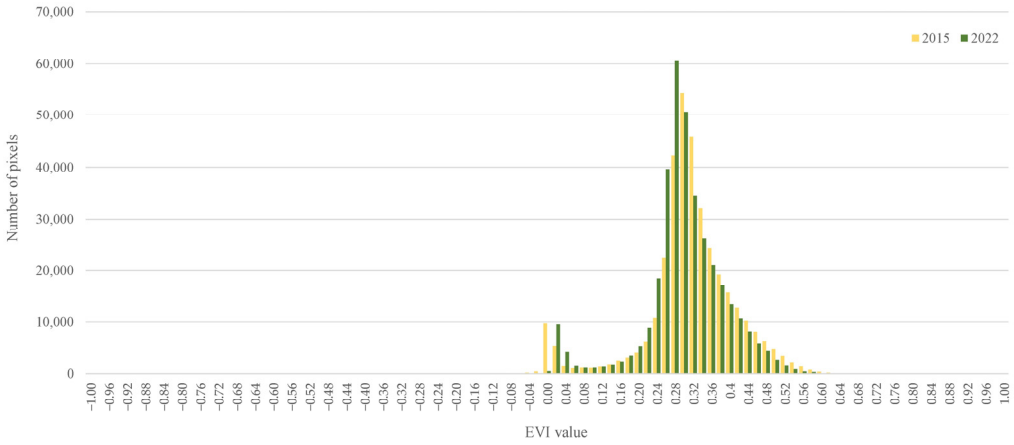

Figure 9. Histogram of the EVI values for the 2015 and for the 2022 data.

The analysis of the descriptive statistics for the NDVI and the EVI values point to the general good condition of the rehabilitated post-mining study area. These statistics are also an indication of the potential effect of meteorological drought in Poland in recent years [75] and probable emergence of hydrological drought in the post-mining study area. This phenomenon should be studied in the future. The local changes occurring in the post-mining area undergoing natural landscaping processes are the subject of the spatiotemporal analyses presented in the next sections.

The maps of spatial distribution of NDVI and EVI values for the selected August dates in the 2015–2022 period have been provided in supplementary materials Figures S1 and S2 respectively.

3.2. Spatial Pattern of NDVI and EVI Values

The spatial distribution of mean NDVI and EVI values for the 2015–2022 period are presented in Figures 10a and 10b, respectively. These values were calculated as the arithmetic mean of each raster cell in the time series of the NDVI and EVI data in the selected dates of the month of August. The resulting NDVI and EVI maps show the average values for the 2015–2022 period against the background of the known extent of underground and open pit mining.

The mean NDVI varies from −0.1748 to 0.7832 with an average of 0.5761 and standard deviation of 0.1085. The negative values of mean NDVI (light green) are associated with anthropogenic water bodies and the low positive values with embankments of the larger artificial lakes, roads, buildings, and old mining dumps in the NE and S parts of the post-mining study area.

The highest positive values of NDVI (dark green) represent undisturbed compact forest area in the Nysa Łużycka River valley (S and W parts of the study area) and forest units with the oldest vegetation (>50 years old) located between the rehabilitated open pits and dumps, as well as in the zones of old underground mining (Figures 3a and 10a).

The mean EVI varies from −0.0552 to 0.5937 with an average of 0.2850 and standard deviation of 0.0872. The spatial distribution of EVI values follows the pattern of NDVI and shows greater spatial differentiation than the first index, e.g., in the old forest units (central and northern parts between redeveloped open pits and in river valley in the south). Thus, due to the character of this spectral index it allows for the analysis of the forest spatial structure and condition in greater detail than with NDVI. The negative values of EVI are also associated with anthropogenic water bodies and the low positive values with embankments of the large reservoirs, roads, buildings, and importantly old dumps in the NE and S parts of the post-mining study area. The highest positive values represent undisturbed forest area in the Nysa Łużycka River valley (S part of the study area) and forest units with the oldest vegetation (>50 years) located between rehabilitated open pits and dumps, as well as in a former underground mining zone (Figures 3a and 10b).

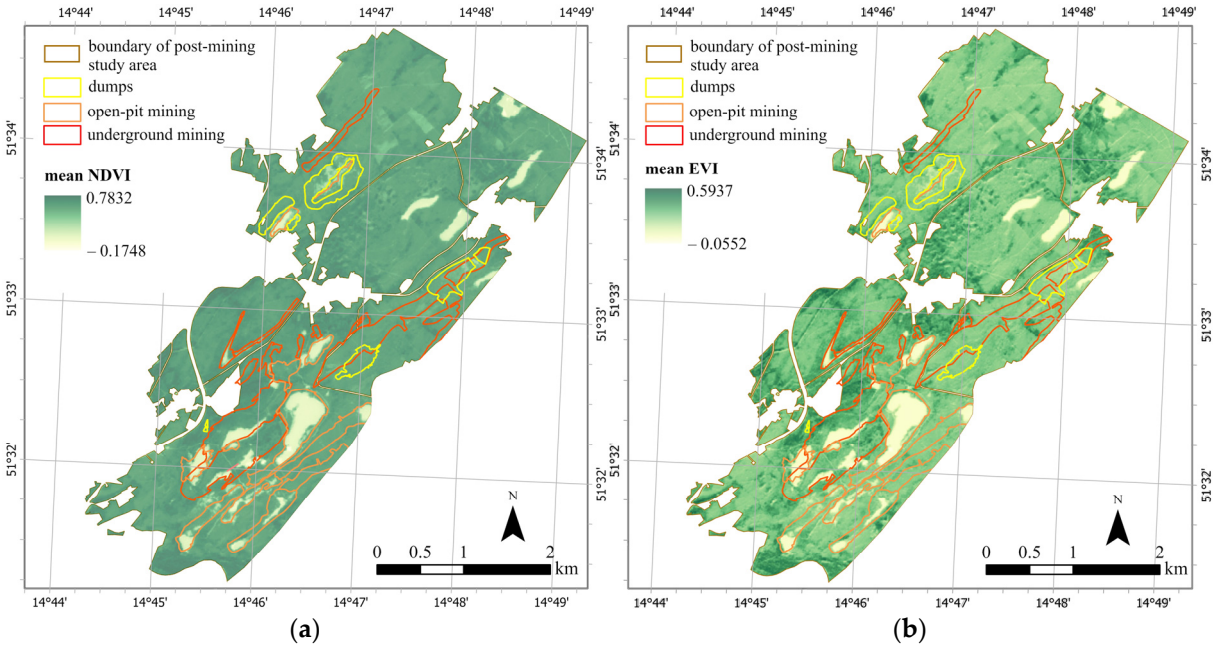

Figure 10. Spatial distribution of mean NDVI (**a**) and mean EVI (**b**) values in the post-mining study area.

The coefficient of variation (CV) maps for the NDVI and EVI spectral indices in the 2015–2022 period, are presented in Figures 11a and 11b respectively. In contrast to Figure 10a,b the latter show the variability of spectral indexes in relation to the mean in the analysed period. Thus, the clusters of higher CV values in local zones indicate that the vegetation cover there varies more strongly than in other places of the rehabilitated post-mining area.

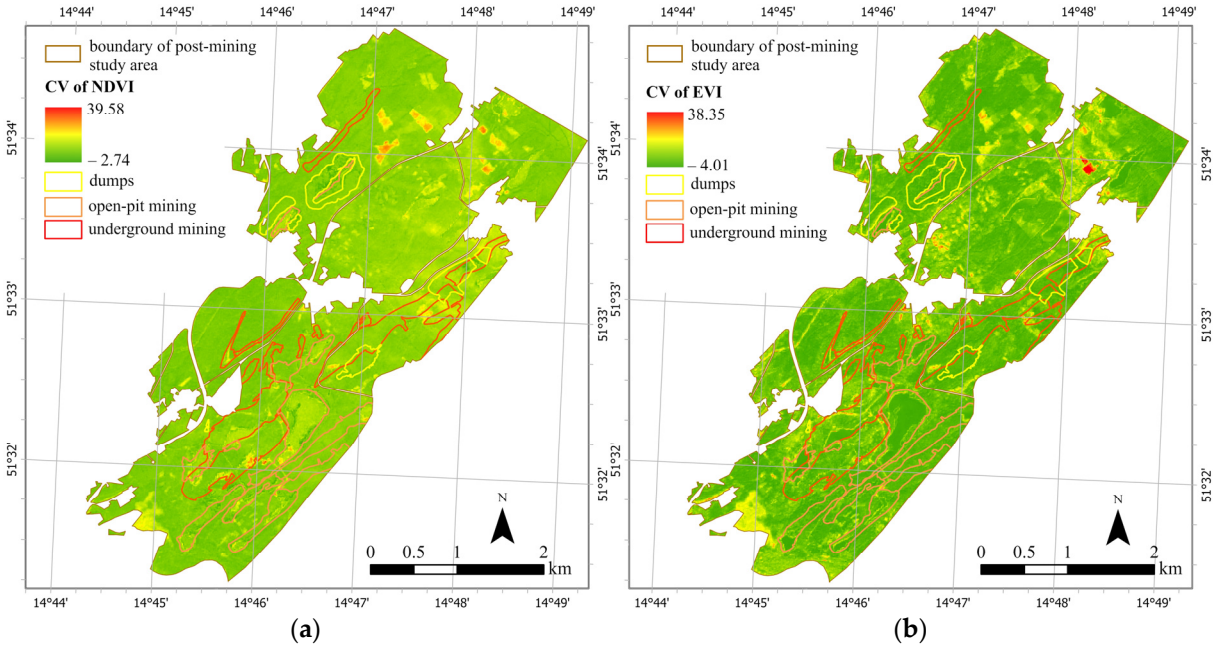

Figure 11. Spatial distribution of CV of NDVI (**a**) and EVI (**b**) in the post-mining study area.

The CV of NDVI varies from −2.74% to 39.58%. The local clusters of high values of CV (orange/red colour) are associated with forest units with the newly planted trees (3 to 6 years) that result from recent forest management activities. There are also local clusters of

high values in the vicinity of anthropogenic water bodies in the southern part of the study area, near water bodies formed above underground mining and along newly constructed trails, e.g., north-west of the largest artificial lake (Figure 11a).

The CV of EVI varies from −4.01% to 38.35% and the spatial distribution follows the pattern of CV of NDVI. The local clusters of high values of CV (orange/red colour) are associated with forest units with the newly planted trees (3 to 6 years) that result from forest management activities. As in the case of NDVI there are local clusters of high values in the vicinity of anthropogenic water bodies in the southern part of the area, near water bodies formed above underground mining and along newly constructed trails (Figure 11b).

3.3. Spatiotemporal Pattern of Hot and Cold Spots

The results of hot spot (HS) and emerging hot spot (EHS) analysis allowed us to identify zones of significant high (hot) and low (cold) values of NDVI and EVI. The hot spot analysis was performed for individual maps representing spectral indexes in the selected dates in August and the emerging hot spot analysis for the entire series of NDVI and EVI data.

The results of hot spot analysis for the final date are shown in Figure 12a for the NDVI data and Figure 12b for the EVI data and present zones of hot and cold spots identified at 99% and 95% confidence level. The largest clusters of cold spots (indicating aggregations of low values of NDVI and EVI) are predominately associated with anthropogenic water bodies. We identified clusters of low values corresponding to barren land areas of waste dumps, large embankments of lakes, as well as emerging vegetation in waterlogged subsidence basins from underground mining (Figure 3a). The latter consists of cold spots identified at 99% (darker blue) and 95% (lighter blue) confidence levels, the former, being water surfaces, predominately 99%.

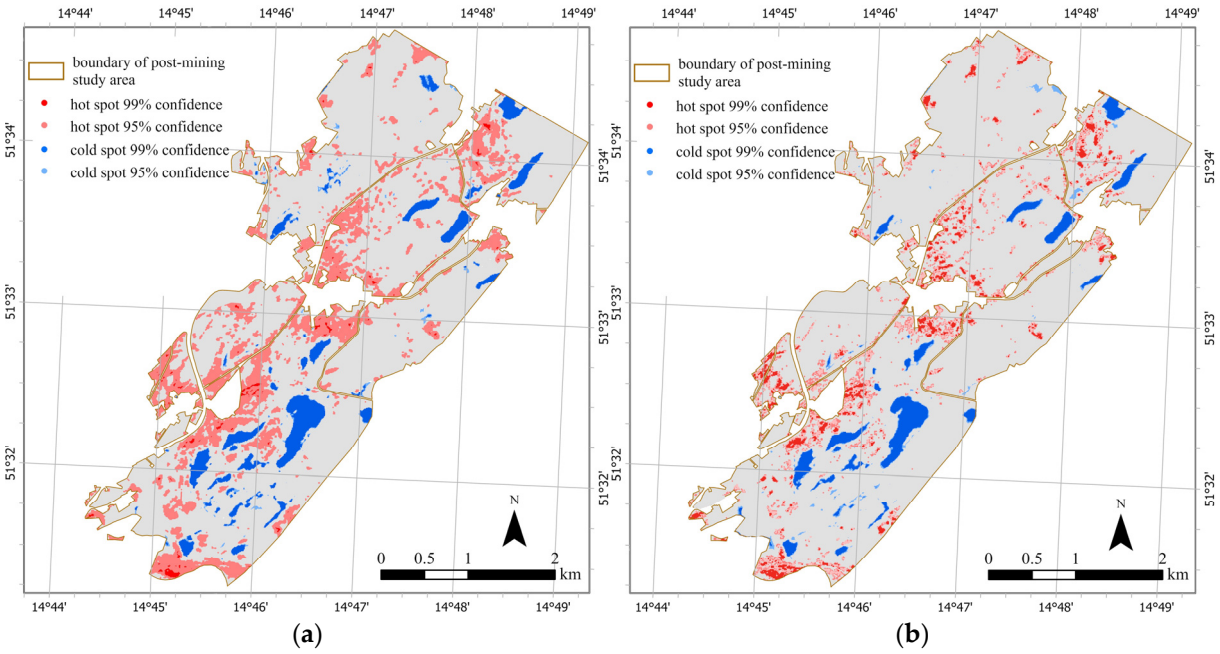

Figure 12. Hot spot pattern of NDVI (**a**) and EVI (**b**) values in the post-mining area in the last year of analysis (2022).

The hot spots, for both the NDVI and EVI, identified in each year of analysis (red clusters) are associated predominately with healthy compact forest zones, areas undisturbed by former mining activity, as well as deciduous forest units. The hot spots identified at 99% and 95% confidence levels are represented by darker and lighter red colours respectively.

Larger areas of hot spots identified at the 95% confidence level for the NDVI than for the EVI, and more local hot spots identified at the 99% confidence level for the EVI are the main differences between the results obtained for both spectral indices.

Next, we applied EHS to analyse the pattern and the trend of vegetation cover condition over time (from 2015 to 2022). The EHS algorithm identifies up to eight types of hot or cold spots described in [76]. Thus, as in the case of HS analysis, clusters of statistically significant low values of NDVI and EVI have been aggregated as cold spots and high values as hot spots. In an analysed time series of data hot or cold spots can intensify or diminish with the variation of vegetation condition.

The spatial pattern of hot and cold spots trends for NDVI and EVI have been shown in Figure 13a and in Figure 13b, respectively. The results of EHS analysis are consistent with the results of HS analysis. However, they provide information on the trajectory of hot and cold spots in time. The statistics of temporal hot and cold spot patterns for NDVI and EVI data in the rehabilitated post-mining area have been shown in Table 4.

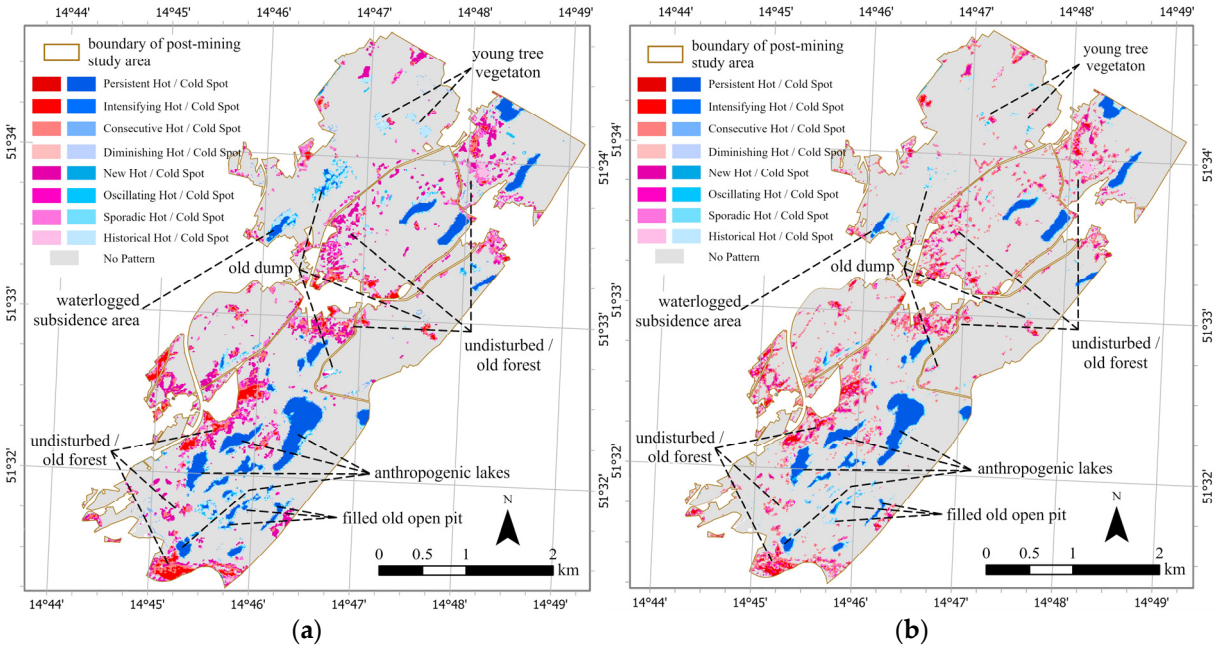

Figure 13. Emerging hot spot pattern of NDVI (**a**) and EVI (**b**) in the rehabilitated post-mining area.

The consecutive, persistent, new and intensifying hot spots are the main observed patterns in case of the NDVI, covering 6.50%, 3.91%, 3.09% and 2.51% of the study area respectively. In the case of the EVI the main observed hot spot patterns include: consecutive (3.37%), new (2.74%), persistent (2.34%) and intensifying (1.19%) of the area.

The cold spot NDVI patterns are predominately persistent (5.87% of the area), new (1.39%), and consecutive (1.02%). Around 1.47% of the area has been classified as a historical hot spot. In the case of the EVI cold spot patterns we identified the persistent (4.29%), new (2.74%) and the historical (1.12%) ones as the most frequent. According to the methodology: a new hot or a cold spot is identified if a location has statistically significant high or low values in the final time bin; a location that has ben statistically significant hot spot for 90 percent of the time-step intervals, including the final time step and the intensity of high values is increasing is classified as an intensifying hot or cold spot; a location that has been a statistically significant hot or cold spot for 90 percent of the time-step intervals without an apparent trend in the intensity of high or low values over time is a persistent hot or cold spot; a location that has been statistically significant hot or cold spot for less than 90 percent of the time-step intervals and the intensity of high or low values in subsequent time steps is decreasing is an diminishing hot or cold spot; a location that has not been a statistically significant hot (cold) spot prior to the final hot (cold) spot run of at least two hot (cold) spot

time-steps and less than 90 percent of all time steps are statistically significant hot (cold) spots is a consecutive hot spot; and a location that has not been a cold spot in at the least the last two time bins. Between 2/3 and 3/4 of the study area has not been identified as statistically significant high or low value of NDVI or EVI respectively in the study period.

Table 4. Emerging hot spot pattern statistics of NDVI and EVI.

Pattern Type	NDVI	NDVI	EVI	EVI
	[km^2]	[%]	[km^2]	[%]
persistent hot spot	0.5389	3.91%	0.3222	2.34%
consecutive hot spot	0.8956	6.50%	0.4648	3.37%
intensifying hot spot	0.3464	2.51%	0.1642	1.19%
diminishing hot spot	0.0300	0.22%	0.0754	0.55%
new hot spot	0.4263	3.09%	0.3778	2.74%
oscillating hot spot	0.1187	0.86%	0.2033	1.48%
sporadic hot spot	0.1831	1.33%	0.0645	0.47%
historical hot spot	0.0370	0.27%	0.0038	0.03%
no pattern	9.6710	70.18%	10.7148	77.75%
persistent cold spot	0.8088	5.87%	0.5906	4.29%
consecutive cold spot	0.1407	1.02%	0.0700	0.51%
intensifying cold spot	0.0246	0.18%	0.0404	0.29%
diminishing cold spot	0.0394	0.29%	0.0382	0.28%
new cold spot	0.1910	1.39%	0.3778	2.74%
oscillating cold spot	0.1231	0.89%	0.1116	0.81%
sporadic cold spot	0.0038	0.03%	0.0071	0.05%
historical cold spot	0.2020	1.47%	0.1539	1.12%

The main difference, in pattern, between the NDVI and EVI is the larger area identified as hot spot pattern in case of the first index. There are more intensifying, persistent sporadic, and especially consecutive hot spots in case of the first one. In case of cold spot patterns, also the area of persistent and consecutive ones is greater for the NDVI data.

This can be attributed to the characteristics of these vegetation indices as EVI corrects the NDVI for soil background noise and is more sensitive in areas with dense vegetation [62,77].

The significant temporal cold spot patterns of NDVI and EVI values are predominately associated with the artificial water bodies, former open pits filled with waste material, and forest units with recently planted trees in place of the ones cut down. The significant temporal hot spot patterns of NDVI and EVI values are associated with undisturbed, older (>40–50 years) forest units and clusters of deciduous tree species. This is particularly visible in case of the EVI data. Representative examples are marked in Figure 13a,b with red colours.

There are local significant positive trend patterns on the shores of artificial lakes (diminishing or oscillating cold spots), in the vicinity of waterlogged areas and parts of the previously barren earth old pits (diminishing cold spots, sporadic and oscillating hot spots).

The distributions of high variation rates are consistent with the distributions of high CV of NDVI and EVI. Figure 14a,b present the significance of NDVI and EVI trends in the rehabilitated post-mining area, respectively.

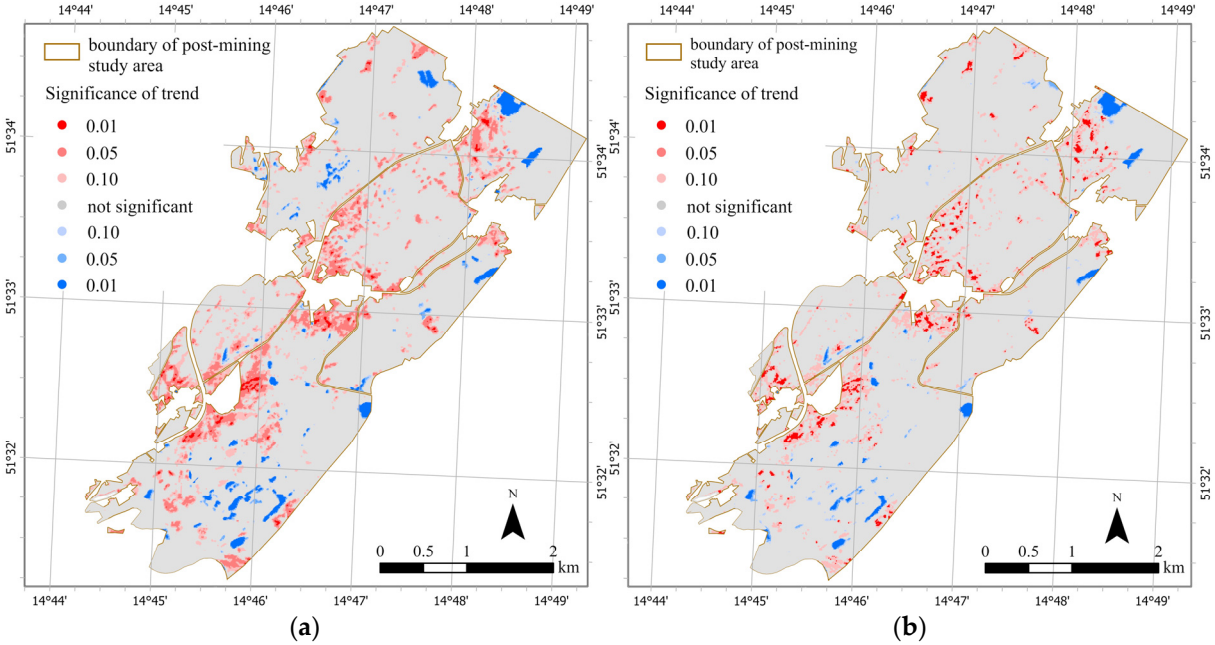

Figure 14. Statistical significance of NDVI (**a**) and EVI (**b**) temporal trends.

3.4. Combinatorial Temporal Class Change Detection

The results of combinatorial class change analysis are presented in Figure 15a for the NDVI and Figure 15b for the EVI. The change of pixel zones from class 1 to higher that happened at a given time step and remained in this class for the remaining time is shown in green colour, the change of pixel zones from higher class to class 1 that happened at a given time step and remained in this class for the remaining time is shown in orange colour. For better clarity the most significant zones of change are marked with red circles, the letters depict field case study sites presented in Figure 16.

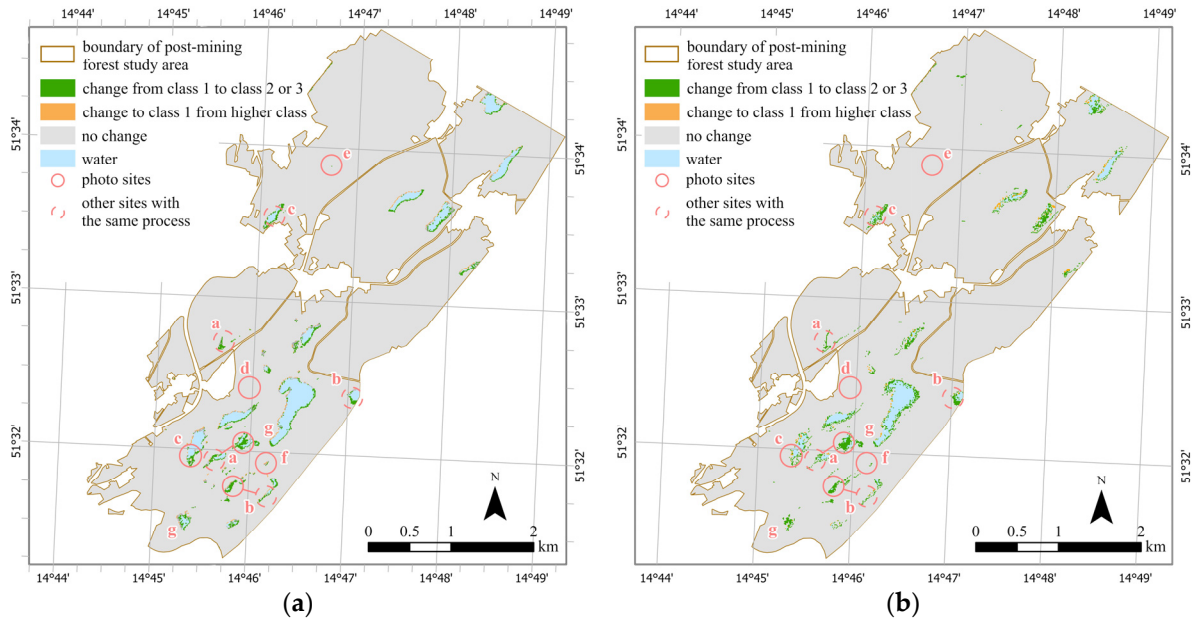

Figure 15. Results of combinatorial class change analysis for the NDVI (**a**) and EVI (**b**).

Figure 16. Site (**a**), vegetation entering borders of subsided flooded area. Site (**b**), low vegetation in a filled and waterlogged former open pit. Site (**c**), dead vegetation in subsided flooded area. Site (**d**), healthy deciduous forest vegetation. Site (**e**), barren land of post-mining dump. Site (**f**), slope of open pit filled with dumped post-mining material.

For the NDVI data, we identified a total area of 0.20 km^2 (1.45%) where vegetation cover condition improved in the analysed time. In case of EVI the positive change occurred over an area of 0.23 km^2 (1.65%). The change from the class representing water (1 in Table 5) and class representing sparse vegetation to healthy vegetation (3 in Table 5) are dominant. The change of class values from 1 to the higher one for both NDVI and EVI is linked to waterlogged areas in former underground mining area, artificial water bodies from open

pit mining that followed underground mining and small artificial water bodies in open pit mining area that experience encroachment of vegetation (Figure 3a, photo shown in Figure 16a). The change to higher class is also associated with open pits filled with material, sometimes partly waterlogged and being gradually overgrown with low vegetation (site b in Figure 15, photo shown in Figure 16b).

Table 5. Combinatorial class change statistics of NDVI and EVI.

Combination	NDVI	EVI
	[km^2]	[km^2]
1	0.0847	0.1373
2	0.0296	0.0042
3	0.0854	0.0864
4	0.0656	0.0288
5	0.0301	0.1572
6	0.0029	0.0000
7	0.4046	0.3551
8	0.0575	0.2099
9	13.0200	12.8015

The opposite change, i.e., from class 2 or 3 to lower class was determined for an area of 0.10 km^2 (0.72%) in case of the NDVI data and an area of 0.19 km^2 (1.35%) in case of the EVI data. The class changes are connected predominately to dumps and embankments of large artificial water bodies and associated with the observed rill erosion of steep slopes [51], as well as human activity, e.g., trail and road construction [78].

Altogether 2.17% and 3.0% of the study area for the NDVI and EVI respectively experienced permanent change of land cover in the analysed period. The remaining area kept their respective classes. These are associated with artificial water bodies and old waste dumps (combinations 7 and 8 in Table 5), e.g., sites c, e and f in Figure 15, and presented in photos (Figure 16c,e,f). The largest unchanged area (combination 9) is associated with forest e.g., site d in Figure 15, photo shown in Figure 16d.

The combinatorial class change detection approach augments results of temporal hot spot analysis and illustrates the permanent changes of land cover type due to landscaping processes occurring locally in the post-mining study area.

3.5. Field Examination

The post-mining area and the zones detected in the combinatorial and Hot Spot analysis were assessed in the field. The selected photographical records of the field reconnaissance are presented in Figure 16a–f. The photos were taken during two field trips on the 15 May 2021 (Figure 16b,e,f) and on the 15 August 2021 (Figure 16a,c,d). The site analysis confirmed the results of the integrated spatiotemporal analysis. We identified sites experiencing encroachment of vegetation in waterlogged (example site a), as well as exposed open pits filled with overburden from open-cast mining operation (example sites c and f). There are zones of barren land in the external waste pits, that are the result of unsuccessful afforestation and have been subjected to natural landscaping processes [79]. These zones experience rill erosion (example site e). Erosion processes occur on the steep embankments of larger artificial lakes.

The underground mining areas experienced ground subsidence that created elongated basins. Some have been waterlogged that led to the dying of vegetation on the surface (example site b). On the other hand, there are also locations with well-developed and healthy coniferous, mixed and deciduous forest in the areas between to old open pits and within underground mining areas (example site d). The average age and type of forest

units in the area are presented in Figures 17a and 17b, respectively. The average age of trees in individual forest units for the former open-pit mining areas range from 20 to 55 years. The forest is younger on waste sites due to secondary reclamation procedures in the 1980'ties [47]. In the areas of former underground mining the tree age ranges from 40 to 70 years. In the areas of combined underground and open-pit mining it is between 20 and 30 years. The typical forest types in the area, according to the National Forest Data Bank nomenclature [80] are: pine forest and mixed coniferous forest, mixed deciduous forest, and deciduous forest, as well as mixed wet forest and riparian forest in the Nysa Łużycka River valley in the south. The most common tree species include the following: pine, birch, oak, spruce, poplar, beech, alder, larch.

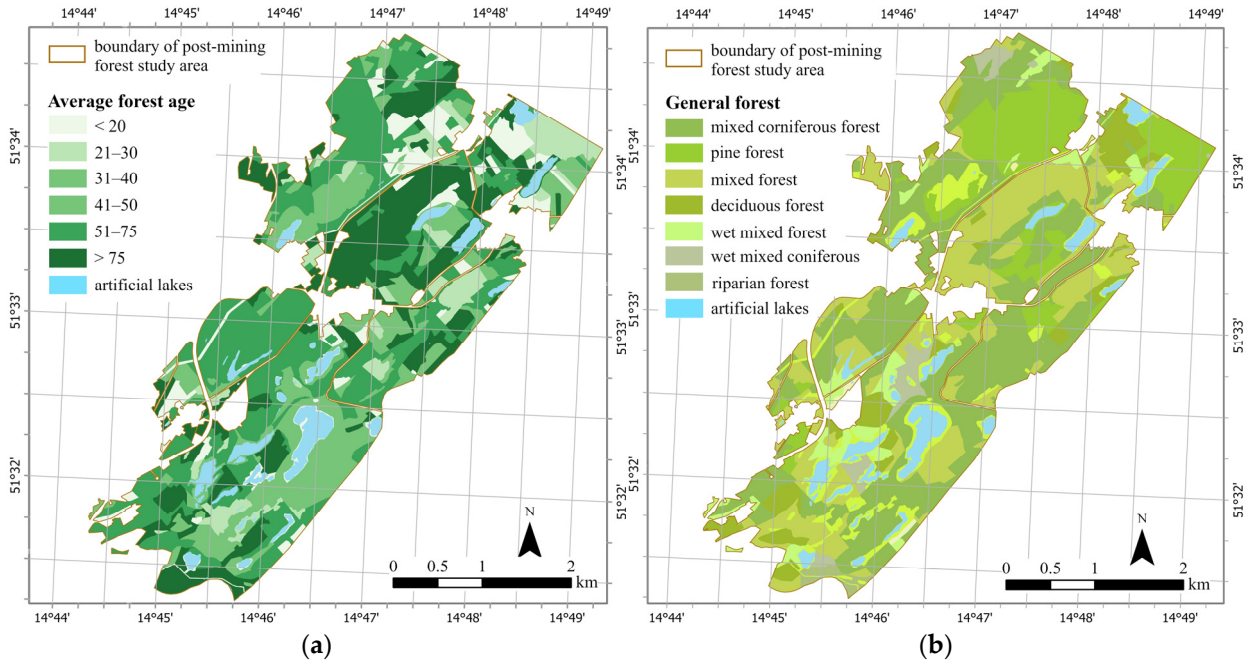

Figure 17. Forest age in units (**a**). Forest types in units (**b**) (after [80]).

The results of spatiotemporal analysis and field investigations point to diverse, both positive and negative landscaping processes in the post-mining areas.

4. Discussion and Comments

The published studies apply and indicate the NDVI as a competent indicator for monitoring vegetation in mining areas, especially for vegetation cover change detection related to starting mining or post-mining recovery processes [9,11,23,24,81]. Nevertheless, we should be aware of the reported deficiencies of this vegetation index such as influence of moisture and the bare soil background on readings [62,77]. Some researchers suggest that it may be worth trying to use it together with other vegetation indices, such as EVI and SAVI, to improve the accuracy [71].

We applied the combination of NDVI and EVI for a study of a rehabilitated lignite post-mining area where forest and artificial water bodies are the dominant land cover types. The EVI is a better indicator of plant stress [61,82,83] and accounts for most of the problems of using the NDVI thus we found it being a good augmentation for analysis of the condition of mixed forest of varied age.

In contrast to many studies that rely on the Landsat data [26,27,30,31,84] we applied the Sentinel-2 imagery. The advantage being the better spatial resolution, the disadvantage being the shorter period of available satellite imagery dating back to 2015. The number of available images, in case of both the Landsat and Sentinel-2 missions, can be reduced due to cloud cover during registration of data. As we have aimed at the analysis of recent

condition of vegetation cover in the area thought to be in the rehabilitated phase, the period of observations (2015–2022) was sufficient for the study. We used images for the month of August to assess vegetation in the same phenological stage. These were available in each year with the exception of 2021 when early September data were used.

We captured the recent general condition of vegetation cover in a rehabilitated post-mining area that resulted from long-term complex underground and open-pit mining of lignite and we were able to confirm the existence of local landscaping processes presently taking place there.

We found the general steady state of forest that was introduced two times, first about five and later four decades ago after unsuccessful initial reclamation [46,47,50]. The combination of spatiotemporal analyses of NDVI and EVI timeseries, temporal Hot Spot and combinatorial class change detection has allowed us to identify locations with improving and worsening condition of vegetation cover. The negative processes include for example the occurrence of barren land on old waste dumps that, as observed during field reconnaissance, undergoes rill erosion. The area of these unvegetated parts did not increase during the 2015–2022 period. The same cannot be said about steep slopes of large artificial water bodies that in several locations experienced deterioration of vegetation as indicated by results of combinatorial and hot spot analysis and confirmed by field study. The other identified processes include slow encroachment of low vegetation in exposed former pits filled with waste rock and encroachment of aquatic vegetation mainly in waterlogged or flooded zones that resulted from subsidence due to underground mining.

Our results show that the post-mining study site is past the recovery stage [9]. However, the areas that were the most transformed by mining still experience processes that need to be further monitored, e.g., with the use of UAV platform. The barren earth zones and dead high vegetation in waterlogged areas provide indication of secondary disturbance that happened years prior to the period of our analysis. The Sentinel-2 resolution proved more than satisfactory for our present study. We should note that reference to a time-series of in situ measurements, e.g., [83], could improve accuracy of our findings but these are not available. Our study is probably the first one aimed at analysis of vegetation cover condition thought to be in the rehabilitated phase in this area. The long-term analysis of recoverying vegetation in this post-mining area based on the mid-spatial resolution of the Landsat imagery was the subject of another publication [85].

In the study we have proposed a methodological approach for the analysis and assessment of the post-mining recovery that can be applied to both short and long time series of remotely sensed data. We have applied a combination of complementary spatiotemporal analysis methods in GIS, temporal hot spot and combinatorial change detection, to obtain a comprehensive portrait of vegetation condition. The hot spot analysis has been applied so far in large scale studies, e.g., river basins or drought areas [66,70–72]. We found it to be an effective method for assessment of vegetation cover condition in a differentiated and complex medium scale post mining area. The reclassification and combinatorial map algebra functions provided a simple and efficient means to detect vegetation condition class change. We have opted for a manual setting of the number of vegetation cover classes, as well as their boundaries based on the analysis of statistics and ground control points. There are other methods available such as cross-correlation analysis, image differencing, object pixel-based classification, post-classification comparison, or image fusion-based change detection [86–89] that can be applied.

A recently applied approach to land use change detection is the LandTrendr algorithm that can be used to identify sudden changes in vegetation condition temporal trajectory for selected locations represented by a stack of pixel data [90,91]. In our case the data timeseries was too short for this analysis and the observed changes are of slow, gradual character. According to Yang et al. [9] it is better suited by open-cast mining which disturbs the terrain to a greater extent than underground mining [92].

The methods proposed and applied for this study can be used in combination or separately in other areas of interest.

5. Conclusions

Post-mining areas, even those thought to be in the rehabilitated phase, require continuous monitoring because of the potential occurrence of secondary disturbances. As has been demonstrated openly available satellite spectral data and a combination of GIS-based spatial statistic methods provide a functional solution for the initial assessment of the condition of vegetation cover prior to or without the need for costly and time-consuming field surveys.

The spatial distribution and temporal trends of NDVI and EVI values indicate that the post-mining study area was generally stable in the 2015–2022 period and past the recovery phase. However, the results of the combinatorial vegetation cover class change and temporal hot spot analyses also showed local disturbances in the condition of land cover. These processes, of both positive and negative character, are the results of secondary disturbances caused by ground subsidence from underground mining, unsuccessful reclamation procedures of waste dumps and slopes of artificial lakes, as well as present-day forest management activities. Our findings prove continouing effects of mining on vegetation even five decades after its ending.

The main local processes of vegetation cover change include, introduction of aquatic vegetation in waterlogged subsidence basins, emergence of low vegetation in old pits filled with waste material, erosion of barren waste dumps and slopes. These are responsible for natural landscaping processes taking place in this, now predominately forest and lake, area of former complex underground and open-pit mining in glacio-tectonic terrain.

The proposed methodology can be used in the most of other post-mining grounds in the world that are in the recovery or rehabilitated phases. Whereas, the monitoring of the Muskau Arch post-mining ground should be continued in the future to assess the trajectory and rate of the identified spatiotemporal trends in vegetation cover condition locally and on the entire study area.

Supplementary Materials: The following supporting information can be downloaded at: https://www.mdpi.com/article/10.3390/rs15123067/s1, Figure S1: NDVI distribution maps; Figure S2: EVI distribution maps.

Author Contributions: Conceptualization J.B.; Methodology, J.B. and S.L.E.; Data analysis, J.B., A.D., A.B. and N.W.; Software, A.D.; Investigation, A.B. and J.B.; Validation, J.B. and S.L.E.; Writing—original draft preparation, J.B. and A.B.; Writing—review and editing, J.B., S.L.E. and A.D.; Visualization, A.D. and J.B.; Supervision, J.B.; Funding acquisition, J.B. All authors have read and agreed to the published version of the manuscript.

Funding: The data acquisition, processing and the field reconnaissance parts were conducted within the frames of the Polish National Science Centre Project no. 2019/33/B/ST10/02975. The analytical part was conducted partly within the frames of the research stay at the Norwegian University of Science and Technology financed by the Polish National Agency for Academic Exchange (NAWA) Bekker programme.

Data Availability Statement: Data available on request from the corresponding author.

Acknowledgments: We wish to thank the Lipinki Forest Management for their assistance, as well as comments of anonymous reviewers that have helped to improve the manuscript.

Conflicts of Interest: The authors declare no conflict of interest.

References

1. Ostręga, A.; Uberman, R. Reclamation and Land Development Directions—Selection Method, Classification and Examples. *Min. Geoengin.* **2010**, *34*, 445–461. (In Polish)
2. Naworyta, W. Once Again about the Directions of Reclamation and Their Choice, Critically. *Min. Sci.* **2013**, *136*, 141–155.
3. Stottmeister, U.; Mudroch, A.; Kennedy, C.; Matiova, Z.; Sanecki, J.; Svoboda, I. Reclamation and Regeneration of Landscapes after Brown Coal Opencast Mining in Six Different Countries. In *Remediation of Abandoned Surface Coal Mining Sites: A NATO-Project*; Mudroch, A., Stottmeister, U., Kennedy, C., Klapper, H., Eds.; Environmental Engineering; Springer: Berlin/Heidelberg, Germany, 2002; pp. 4–36, ISBN 978-3-662-04734-7.

4. Macdonald, S.E.; Landhäusser, S.M.; Skousen, J.; Franklin, J.; Frouz, J.; Hall, S.; Jacobs, D.F.; Quideau, S. Forest Restoration Following Surface Mining Disturbance: Challenges and Solutions. *New For.* **2015**, *46*, 703–732. [CrossRef]
5. Molenda, T. Mining anthropogenic environments—objects of observation of geomorphological and biological processes (on the example of the Silesian Voivodeship). *Sci. Work. Min. Inst. Wrocław Univ. Sci. Technol.* **2005**, *111*, 187–196. (In Polish)
6. Myga-Piątek, U. Landscape Management on Post-Exploitation Land Using the Example of the Silesian Region, Poland. *Environ. Socio-Econ. Stud.* **2014**, *2*, 1–8. [CrossRef]
7. Kretschmann, J.; Nguyen, N. Research Areas in Post-Mining—Experiences from German Hard Coal Mining. *J. Pol. Miner. Eng. Soc.* **2020**, *1*, 255–262. [CrossRef]
8. Rudolph, T.; Goerke-Malle, P.; Melchers, C. Geomonitoring Im Alt- Und Nachbergbau. *ZfV-Z. Geodäsie Geoinf. Landmanag.* **2020**, *33*, 168–173. (In German) [CrossRef]
9. Yang, Y.; Erskine, P.D.; Lechner, A.M.; Mulligan, D.; Zhang, S.; Wang, Z. Detecting the Dynamics of Vegetation Disturbance and Recovery in Surface Mining Area via Landsat Imagery and LandTrendr Algorithm. *J. Clean. Prod.* **2018**, *178*, 353–362. [CrossRef]
10. Blachowski, J.; Kopeć, A.; Milczarek, W.; Owczarz, K. Evolution of Secondary Deformations Captured by Satellite Radar Interferometry: Case Study of an Abandoned Coal Basin in SW Poland. *Sustainability* **2019**, *11*, 884. [CrossRef]
11. Bao, N.; Lechner, A.; Fletcher, A.; Erskine, P.; Mulligan, D.; Bai, Z. SPOTing Long-Term Changes in Vegetation over Short-Term Variability. *Int. J. Min. Reclam. Environ.* **2014**, *28*, 2–24. [CrossRef]
12. Latifovic, R.; Fytas, K.; Chen, J.; Paraszczak, J. Assessing Land Cover Change Resulting from Large Surface Mining Development. *Int. J. Appl. Earth Obs. Geoinf.* **2005**, *7*, 29–48. [CrossRef]
13. Firozjaei, M.K.; Sedighi, A.; Firozjaei, H.K.; Kiavarz, M.; Homaee, M.; Arsanjani, J.J.; Makki, M.; Naimi, B.; Alavipanah, S.K. A Historical and Future Impact Assessment of Mining Activities on Surface Biophysical Characteristics Change: A Remote Sensing-Based Approach. *Ecol. Indic.* **2021**, *122*, 107264. [CrossRef]
14. Bandopadhyay, S.; Rastogi, A.; Juszczak, R. Review of Top-of-Canopy Sun-Induced Fluorescence (SIF) Studies from Ground, UAV, Airborne to Spaceborne Observations. *Sensors* **2020**, *20*, 1144. [CrossRef] [PubMed]
15. Bannari, A.; Morin, D.; Bonn, F.; Huete, A.R. A Review of Vegetation Indices. *Remote Sens. Rev.* **1995**, *13*, 95–120. [CrossRef]
16. Pearson, R.L.; Miller, L.D. *Remote Mapping of Standing Crop Biomass for Estimation of the Productivity of the Shortgrass Prairie, Pawnee National Grasslands, Colorado*; Environmental Research Institution of Michigan: Ann Arbor, MI, USA, 1972; p. 1355.
17. Qi, J.; Chehbouni, A.; Huete, A.R.; Kerr, Y.H.; Sorooshian, S. A Modified Soil Adjusted Vegetation Index. *Remote Sens. Environ.* **1994**, *48*, 119–126. [CrossRef]
18. Plummer, S.E.; North, P.R.; Briggs, S.A. *The Angular Vegetation Index: An Atmospherically Resistant Index for the Second along Track Scanning Radiometer (ATSR-2)*; ISPRS: Val d'Isère, France, 1994.
19. Xue, J.; Su, B. Significant Remote Sensing Vegetation Indices: A Review of Developments and Applications. *J. Sens.* **2017**, *2017*, 1353691. [CrossRef]
20. Henrich, V.; Krauss, G.; Götze, C.; Sandow, C. IDB—Entwicklung Einer Datenbank Für Fernerkundungsindizes. 2012. Available online: www.Indexdatabase.de (accessed on 22 September 2022). (In German).
21. Pawlik, M.; Rudolph, T.; Benndorf, J.; Blachowski, J. Review of Vegetation Indices for Studies of Post-Mining Processes. *IOP Conf. Ser. Earth Environ. Sci.* **2021**, *942*, 012034. [CrossRef]
22. Buczyńska, A. Badania Studies of components of the natural environment on post-mining areas with using high-resolution satellite imagery. *Min. Rev.* **2020**, *1168*, 1–8. (In Polish)
23. Zipper, C.; Donovan, P.; Wynne, R.; Oliphant, A. Character Analysis of Mining Disturbance and Reclamation 786 Trajectory in Surface Coal-Mine Area by Time-Series NDVI. *Nongye Gongcheng Xuebao/Trans. Chin. Soc. Agric. Eng.* **2015**, *31*, 251–257.
24. Karan, S.K.; Samadder, S.R.; Maiti, S.K. Assessment of the Capability of Remote Sensing and GIS Techniques for Monitoring Reclamation Success in Coal Mine Degraded Lands. *J. Environ. Manag.* **2016**, *182*, 272–283. [CrossRef]
25. Yao, Z.; Wei, Z. Correlation Analysis between Vegetation Fraction and Vegetation Indices in Reclaimed Forest: A Case Study in Pingshuo Mining Area. In Proceedings of the 2016 4th International Workshop on Earth Observation and Remote Sensing Applications (EORSA), Guangzhou, China, 4–6 July 2016; pp. 122–126.
26. Padmanaban, R.; Bhowmik, A.; Cabral, P. A Remote Sensing Approach to Environmental Monitoring in a Reclaimed Mine Area. *ISPRS Int. J. Geo-Inf.* **2017**, *6*, 401. [CrossRef]
27. Li, H.; Lei, J.; Wu, J. Analysis of Land Damage and Recovery Process in Rare Earth Mining Area Based on Multi-Source Sequential NDVI. *Nongye Gongcheng Xuebao/Trans. Chin. Soc. Agric. Eng.* **2018**, *34*, 232–240.
28. Wu, Q.; Liu, K.; Song, C.; Wang, J.; Ke, L.; Ma, R.; Zhang, W.; Pan, H.; Deng, X. Remote Sensing Detection of Vegetation and Landform Damages by Coal Mining on the Tibetan Plateau. *Sustainability* **2018**, *10*, 3851. [CrossRef]
29. Kopeć, A.; Trybała, P.; Głąbicki, D.; Buczyńska, A.; Owczarz, K.; Bugajska, N.; Kozińska, P.; Chojwa, M.; Gattner, A. Application of Remote Sensing, GIS and Machine Learning with Geographically Weighted Regression in Assessing the Impact of Hard Coal Mining on the Natural Environment. *Sustainability* **2020**, *12*, 9338. [CrossRef]
30. Vidal-Macua, J.J.; Nicolau, J.M.; Vicente, E.; Moreno-de las Heras, M. Assessing Vegetation Recovery in Reclaimed Opencast Mines of the Teruel Coalfield (Spain) Using Landsat Time Series and Boosted Regression Trees. *Sci. Total Environ.* **2020**, *717*, 137250. [CrossRef]
31. Vorovencii, I. Changes Detected in the Extent of Surface Mining and Reclamation Using Multitemporal Landsat Imagery: A Case Study of Jiu Valley, Romania. *Environ. Monit. Assess.* **2021**, *193*, 30. [CrossRef]

32. Guan, Y.; Wang, J.; Zhou, W.; Bai, Z.; Cao, Y. Identification of Land Reclamation Stages Based on Succession Characteristics of Rehabilitated Vegetation in the Pingshuo Opencast Coal Mine. *J. Environ. Manag.* **2022**, *305*, 114352. [CrossRef] [PubMed]
33. Huang, S.; Tang, L.; Hupy, J.P.; Wang, Y.; Shao, G. A Commentary Review on the Use of Normalized Difference Vegetation Index (NDVI) in the Era of Popular Remote Sensing. *J. For. Res.* **2021**, *32*, 1–6. [CrossRef]
34. Blachowski, J. Application of GIS Spatial Regression Methods in Assessment of Land Subsidence in Complicated Mining Conditions: Case Study of the Walbrzych Coal Mine (SW Poland). *Nat. Hazards* **2016**, *84*, 997–1014. [CrossRef]
35. Sawut, R.; Kasim, N.; Abliz, A.; Hu, L.; Yalkun, A.; Maihemuti, B.; Qingdong, S. Possibility of Optimized Indices for the Assessment of Heavy Metal Contents in Soil around an Open Pit Coal Mine Area. *Int. J. Appl. Earth Obs. Geoinf.* **2018**, *73*, 14–25. [CrossRef]
36. Cao, J.; Ma, F.; Guo, J.; Lu, R.; Liu, G. Assessment of Mining-Related Seabed Subsidence Using GIS Spatial Regression Methods: A Case Study of the Sanshandao Gold Mine (Laizhou, Shandong Province, China). *Environ. Earth Sci.* **2019**, *78*, 26. [CrossRef]
37. Petropoulos, G.P.; Partsinevelos, P.; Mitraka, Z. Change Detection of Surface Mining Activity and Reclamation Based on a Machine Learning Approach of Multi-Temporal Landsat TM Imagery. *Geocarto Int.* **2013**, *28*, 323–342. [CrossRef]
38. Chen, Y.; Luo, M.; Xu, L.; Zhou, X.; Ren, J.; Zhou, J. Object-Based Random Forest Classification of Land Cover from Remotely Sensed Imagery for Industrial and Mining Reclamation. *Int. Arch. Photogramm. Remote Sens. Spat. Inf. Sci.* **2018**, *XLII–3*, 199–206. [CrossRef]
39. Zhang, M.; Zhou, W.; Li, Y. The Analysis of Object-Based Change Detection in Mining Area: A Case Study with Pingshuo Coal. *ISPRS Int. Arch. Photogramm. Remote Sens. Spat. Inf. Sci.* **2017**, *XLII-2/W7*, 1017–1023. [CrossRef]
40. LeClerc, E.; Wiersma, Y. Assessing Post-Industrial Land Cover Change at the Pine Point Mine, NWT, Canada Using Multi-Temporal Landsat Analysis and Landscape Metrics. *Environ. Monit. Assess.* **2017**, *189*, 185. [CrossRef]
41. Szostak, M.; Knapik, K.; Wężyk, P.; Likus-Cieślik, J.; Pietrzykowski, M. Fusing Sentinel-2 Imagery and ALS Point Clouds for Defining LULC Changes on Reclaimed Areas by Afforestation. *Sustainability* **2019**, *11*, 1251. [CrossRef]
42. European Space Agency User Guides—Sentinel-2 MSI—Sentinel Online—Sentinel Online. Available online: https://sentinels.copernicus.eu/web/sentinel/user-guides/sentinel-2-msi (accessed on 22 September 2022).
43. Dyjor, S.; Chlebowski, Z. Geological structure of the Polish part of the Muskau Arch. *Acta. Univ. Wratislaviensis. Pr. Geol.-Miner.* **1973**, *192*, 3–41. (In Polish)
44. Kupetz, M. Geologischer Bau Und Genese Der Stauchendmoräne Muskauer Faltenbogen. *Brandenbg. Geowiss. Beiträge* **1973**, *2*, 1–20. (In German)
45. Koźma, J. Anthropogenic landscape changes connected with the old brown coal mining based on the example of the polish part of the Muskau arch area. *Opencast Min.* **2016**, *57*, 5–13. (In Polish)
46. Greinert, H.; Drab, M.; Greinert, A. *Studies on the Effectiveness of Forest Restoration of the Phytotoxic Acid Miocene Sands Dumps of the Former Lignite Mine in Łęknica*; Publishing House of the University of Zielona Góra: Zielona Góra, Poland, 2009; ISBN 978-83-7481-220-7. (In Polish)
47. Greinert, A.; Bazan-Krzywoszańska, A.; Drab, M.; Fiszer, J.; Gontaszewska, A.; Jachimko, B.; Jędrczak, A.; Kraiński, A.; Krzaklewski, W.; Maciantowicz, M.; et al. *Lignite Mining and Reclamation of Post-Mining Areas in the Lubuskie Region*; Institute of Environmental Engineering of the University of Zielona Góra: Zielona Góra, Poland, 2015; ISBN 978-83-937619-2-0. (In Polish)
48. Kasiński, J.R.; Słodkowska, B. Lignite seams in the Muskau arch—sedimentation conditions, stratigraphic position, deposits importance. *Opencast Min.* **2017**, *58*, 20–31. (In Polish)
49. Oszkinis-Golon, M.; Frankowski, M.; Jerzak, L.; Pukacz, A. Physicochemical Differentiation of the Muskau Arch Pit Lakes in the Light of Long-Term Changes. *Water* **2020**, *12*, 2368. [CrossRef]
50. Koźma, J. Analysis of the Landscape Evolution of the Polish Part of the Muskau Arch and Its Valorisation in the Aspect of Protection of Geological Heritage. Ph.D. Dissertation, The Polish Geological Institute—National Research Institute, Kraków, Poland, 2018.
51. Blachowski, J.; Warchala, E.; Koźma, J.; Buczyńska, A.; Bugajska, N.; Becker, M.; Janicki, D.; Kujawa, P.; Kwaśny, L.; Wajs, J.; et al. Geophysical Research of Secondary Deformations in the Post Mining Area of the Glaciotectonic Muskau Arch Geopark—Preliminary Results. *Appl. Sci.* **2022**, *12*, 1194. [CrossRef]
52. Suhet; Hoersch, B. *Sentinel-2 User Handbook*; European Space Agency: Paris, France, 2015.
53. Mueller-Wilm, U.; Devignot, O.; Pessiot, L. *S2 MPC Sen2Cor Configuration and User Manual*; European Space Agency: Paris, France, 2020; pp. 1–56.
54. Matejicek, L.; Kopackova, V. Changes in Croplands as a Result of Large Scale Mining and the Associated Impact on Food Security Studied Using Time-Series Landsat Images. *Remote Sens.* **2010**, *2*, 1463. [CrossRef]
55. Zhu, X.; Zhou, Y.; Yang, Y.; Hou, H.; Zhang, S.; Liu, R. Estimation of the Restored Forest Spatial Structure in Semi-Arid Mine Dumps Using Worldview-2 Imagery. *Forests* **2020**, *11*, 695. [CrossRef]
56. Rouse, J.W.; Haas, R.H.; Schell, J.A.; Deering, D.W. *Monitoring Vegetation Systems in the Great Plains with ERTS*; NASA: Washington, DC, USA, 1974.
57. Tucker, C. Red and Photographic Infrared Linear Combinations for Monitoring Vegetation. *Remote Sens. Environ.* **1979**, *8*, 127–150. [CrossRef]
58. Myneni, R.B.; Hall, F.G.; Sellers, P.J.; Marshak, A.L. The Interpretation of Spectral Vegetation Indexes. *IEEE Trans. Geosci. Remote Sens.* **1995**, *33*, 481–486. [CrossRef]

59. Zhang, J.; Zhang, L.; Xu, C.; Liu, W.; Qi, Y.; Wo, X. Vegetation Variation of Mid-Subtropical Forest Based on MODIS NDVI Data—A Case Study of Jinggangshan City, Jiangxi Province. *Acta Ecol. Sin.* **2014**, *34*, 7–12. [CrossRef]
60. Gamon, J.; Field, C.; Goulden, M.; Griffin, K.; Hartley, A.; Joel, G.; Penuelas, J.; Valentini, R. Relationships Between NDVI, Canopy Structure, and Photosynthesis in Three Californian Vegetation Types. *Ecol. Appl.* **1995**, *5*, 28–41. [CrossRef]
61. Huete, A.; Didan, K.; Miura, T.; Rodriguez, E.P.; Gao, X.; Ferreira, L.G. Overview of the Radiometric and Biophysical Performance of the MODIS Vegetation Indices. *Remote Sens. Environ.* **2002**, *83*, 195–213. [CrossRef]
62. Pettorelli, N. *The Normalized Difference Vegetation Index*; OUP Oxford: Oxford, UK, 2014; ISBN 978-0-19-969316-0.
63. Bari, E.; Nipa, N.J.; Roy, B. Association of Vegetation Indices with Atmospheric & Biological Factors Using MODIS Time Series Products. *Environ. Chall.* **2021**, *5*, 100376. [CrossRef]
64. Tomlin, D. *Geographic Information Systems and Cartographic Modeling*; Prentice Hall: Hoboken, NJ, USA, 1990; ISBN 978-0-13-350927-4.
65. Statsoft Electronic Statistics Textbook. Available online: https://www.statsoft.pl/textbook/stathome.html (accessed on 3 February 2023).
66. Xu, B.; Qi, B.; Ji, K.; Liu, Z.; Deng, L.; Jiang, L. Emerging Hot Spot Analysis and the Spatial–Temporal Trends of NDVI in the Jing River Basin of China. *Environ. Earth Sci.* **2022**, *81*, 55. [CrossRef]
67. Getis, A.; Ord, J.K. The Analysis of Spatial Association by Use of Distance Statistics. *Geogr. Anal.* **1992**, *24*, 189–206. [CrossRef]
68. Ord, J.K.; Getis, A. Local Spatial Autocorrelation Statistics: Distributional Issues and an Application. *Geogr. Anal.* **1995**, *27*, 286–306. [CrossRef]
69. ESRI How Hot Spot Analysis (Getis-Ord Gi*) Works—ArcGIS Pro | Documentation. Available online: https://pro.arcgis.com/en/pro-app/2.8/tool-reference/spatial-statistics/h-how-hot-spot-analysis-getis-ord-gi-spatial-stati.htm (accessed on 22 September 2022).
70. Nallan, S.A.; Armstrong, L.J.; Tripathy, A.K.; Teluguntla, P. *Hot Spot Analysis Using NDVI Data for Impact Assessment of Watershed Development*; IEEE: Mumbai, India, 2015; pp. 1–5.
71. Zhang, L.; Luo, H.; Zhang, X. Land-Greening Hotspot Changes in the Yangtze River Economic Belt during the Last Four Decades and Their Connections to Human Activities. *Land* **2022**, *11*, 605. [CrossRef]
72. Nejadrekabi, M.; Eslamian, S.; Zareian, M.J. Spatial Statistics Techniques for SPEI and NDVI Drought Indices: A Case Study of Khuzestan Province. *Int. J. Environ. Sci. Technol.* **2022**, *19*, 6573–6594. [CrossRef]
73. Fraser, R.H.; Li, Z.; Cihlar, J. Hotspot and NDVI Differencing Synergy (HANDS): A New Technique for Burned Area Mapping over Boreal Forest. *Remote Sens. Environ.* **2000**, *74*, 362–376. [CrossRef]
74. StatSoft Electronic Manual of Statistics. Available online: https://www.statsoft.pl/textbook/stathome.html (accessed on 22 September 2022). (In Polish).
75. ADMS—Agricultural Drought Monitoring System. Available online: https://susza.iung.pulawy.pl/en (accessed on 3 February 2023).
76. ESRI How Emerging Hot Spot Analysis Works—ArcGIS Pro | Documentation. Available online: https://pro.arcgis.com/en/pro-app/latest/tool-reference/space-time-pattern-mining/learnmoreemerging.htm (accessed on 22 September 2022).
77. Jones, J.R.; Fleming, C.S.; Pavuluri, K.; Alley, M.M.; Reiter, M.S.; Thomason, W.E. Influence of Soil, Crop Residue, and Sensor Orientations on NDVI Readings. *Precis. Agric* **2015**, *16*, 690–704. [CrossRef]
78. Bartkowiak, K. Analysis of the Relationship between the State of Vegetation and Former Mining Activity in a Selected Area of the Former Mine "Przyjaźń Narodów—Shaft Babina. Master's Thesis, Wroclaw University of Science and Technology, Wroclaw, Poland, 2021, (In Polish, unpublished).
79. Schulz, F.; Wiegleb, G. Development Options of Natural Habitats in a Post-Mining Landscape. *Land Degrad. Dev.* **2000**, *11*, 99–110. [CrossRef]
80. National Forest—Forest Data Bank. Available online: https://www.bdl.lasy.gov.pl/portal/mapy-en (accessed on 22 September 2022).
81. Liu, X.; Zhou, W.; Bai, Z. Vegetation coverage change and stability in large open-pit coal mine dumps in China during 1990—2015. *Ecol. Eng.* **2016**, *95*, 447–451. [CrossRef]
82. Pettorelli, N.; Vik, J.O.; Mysterud, A.; Gaillard, J.-M.; Tucker, C.J.; Stenseth, N.C. Using the Satellite-Derived NDVI to Assess Ecological Responses to Environmental Change. *Trends Ecol. Evol.* **2005**, *20*, 503–510. [CrossRef]
83. Glenn, E.P.; Huete, A.R.; Nagler, P.L.; Nelson, S.G. Relationship Between Remotely-Sensed Vegetation Indices, Canopy Attributes and Plant Physiological Processes: What Vegetation Indices Can and Cannot Tell Us About the Landscape. *Sensors* **2008**, *8*, 2136–2160. [CrossRef]
84. Erener, A. Remote sensing of vegetation health for reclaimed areas of Seyitömer open cast coal mine. *Int. J. Coal Geol.* **2011**, *86*, 20–26. [CrossRef]
85. Buczyńska, A.; Blachowski, J.; Bugajska-Jędraszek, N. Analysis of Post-Mining Vegetation Development Using Remote Sensing and Spatial Regression Approach: A Case Study of Former Babina Mine (Western Poland). *Remote Sens.* **2023**, *15*, 719. [CrossRef]
86. Yang, Z.; Zhang, Z.; Zhang, T.; Fahad, S.; Cui, K.; Nie, L.; Peng, S.; Huang, J. The Effect of Season-Long Temperature Increases on Rice Cultivars Grown in the Central and Southern Regions of China. *Front. Plant Sci.* **2017**, *8*, 1908. [CrossRef]
87. Birhanu, A.; Masih, I.; van der Zaag, P.; Nyssen, J.; Cai, X. Impacts of land use and land cover changes on hydrology of the Gumara catchment, Ethiopia. *Phys. Chem. Earth Parts A/B/C* **2019**, *112*, 165–174. [CrossRef]

88. Lucas, R.; Rowlands, A.; Brown, A.; Keyworth, S.; Bunting, P. Rule-based classification of multi-temporal satellite imagery for habitat and agricultural land cover mapping. *ISPRS J. Photogramm. Remote Sens.* **2007**, *62*, 165–185. [CrossRef]
89. Hu, Y.; Raza, A.; Syed, N.R.; Acharki, S.; Ray, R.L.; Hussain, S.; Dehghanisanij, H.; Zubair, M.; Elbeltagi, A. Land Use/Land Cover Change Detection and NDVI Estimation in Pakistan's Southern Punjab Province. *Sustainability* **2023**, *15*, 3572. [CrossRef]
90. Kennedy, R.E.; Yang, Z.; Cohen, W.B. Detecting Trends in Forest Disturbance and Recovery Using Yearly Landsat Time Series: 1. LandTrendr—Temporal Segmentation Algorithms. *Remote Sens. Environ.* **2010**, *114*, 2897–2910. [CrossRef]
91. Liu, Y.; Xie, M.; Liu, J.; Wang, H.; Chen, B. Vegetation Disturbance and Recovery Dynamics of Different Surface Mining Sites via the LandTrend Algorithm: Case Study in Inner Mongolia, China. *Land* **2022**, *11*, 856. [CrossRef]
92. Lechner, A.M.; Baumgartl, T.; Matthew, P.; Glenn, V. The Impact of Underground Longwall Mining on Prime Agricultural Land: A Review and Research Agenda. *Land Degrad. Dev.* **2016**, *27*, 1650–1663. [CrossRef]